ELECTROCHEMICAL SCREENING AND SURFACE ANALYSIS OF ENVIRONMENTALLY FRIENDLY CORROSION INHIBITORS FOR AEROSPACE ALUMINIUM ALLOY.

MASTER THESIS

- Parth SEWLIKAR

ELECTROCHEMICAL SCREENING AND SURFACE ANALYSIS OF ENVIRONMENTALLY FRIENDLY CORROSION INHIBITORS FOR AEROSPACE ALUMINIUM ALLOY.

MASTER THESIS

Thesis

submitted to the

Delft University of Technology

in partial fulfillment of the requirements for the degree of

Master of Science in Materials Science and Engineering

by

Parth SEWLIKAR

March 2022, Delft

Keywords: Corrosion, corrosion inhibitors, aerospace aluminium alloys, organic and inorganic compounds, electrochemistry, surface studies, potentiodynamic polarisation, electrochemical impedance spectroscopy, linear polarisation resistance, fourier transform infrared spectroscopy, x-ray photoelectron spectroscopy, time dependence, inhibitor screening and performance, inhibitor efficiency, correlation of methods

Supervisor: Dr. Peyman Taheri

Supervisor: Ir. Can Özkan

Co-readers: Dr. Poulumi Dey
Dr. Ursa Tiringer

To my parents, Dr. Vinayak Sewlikar and Manisha Sewlikar

ACKNOWLEDGEMENTS

It is with great pleasure that I write this section to express my gratitude to everyone who have contributed to this research directly or indirectly and made this project a memorable one.

First and foremost, I am grateful to my supervisor and chair, Dr. Peyman Taheri to give me this opportunity to work on such novel project and support me throughout my work. Your insights on the projects and clear approach has helped me steer in the right direction, always. I would also like to thank my daily supervisor, Ir. Can Özkan, for being so patient with me and guiding me from the beginning, in every small steps. I remember the day when we started our own journeys together, right in front of the XPS lab. From that time until today, I look upon you as a wonderful mentor and friend. Besides my supervisors, I am particularly grateful to Dr. Poulumi Dey and Dr. Ursa Tiringer for taking your time out and being in my defense committee. I gratefully acknowledge Dr. Arjan Mol and Dr. Yaiza Garcia Gonzales, for their support in finding me this thesis topic and directing me to work in this area.

Special thanks to our skilled technician, Agnieszka Kooijman, who trained me with the laboratory experiments, and for keeping me safe while working with chemicals. I will miss the 'liquid nitrogen fill-up' sessions we had during experiments. I wont miss the opportunity to thank Dr. Ali Kosari, Dr. Mirsajjad Mousavi and everyone from the laboratory, for all the times you have helped me during experiments. It is because of experts like you that we have such a wonderful 'electrochemistry' research group.

Next, I would like to thank my father, Dr. Vinayak Sewlikar, for his infinite encouragement and support throughout my academic career, and always pushing me to achieve something great. Also, my mother, Manisha Sewlikar, for all the sacrifices and care. I am blessed to have such strong foundations. At the same time, I acknowledge my grandparents, and everyone in the family, for their constant moral support throughout my work.

I am deeply grateful to all my colleagues and friends, at TU Delft for making this MSc journey as enjoyable as possible, despite the strange circumstances. In addition, special thanks to my room-mates, Himani, Saurabh and Shaurya for being my mini-family at Delft, and for all the wonderful dinners and movie sessions we have had. Lastly, I would like to thank all my friends from India and different parts of the globe, for all the delightful phone calls and regularly checking on me. This thesis wouldn't have completed without your loving support.

ABSTRACT

For the past few decades, the aerospace industry has been actively looking for measures to tackle the problem of localized corrosion of aluminium alloy 2024-T3. One such measure was the use of hexavalent chromium salts as corrosion inhibitors. However, recent studies have reflected the environmental concerns and health impacts associated with these compounds. Since then, there has been a quest for alternatives that can be used as corrosion inhibitors for AA2024-T3. This thesis is aimed at studying these compounds by testing their inhibitive properties.

Selecting an inhibitor from a set of compounds and recommending the best one is a crucial process. The research focuses on the screening of these inhibitors through various electrochemical techniques such as Potentiodynamic Polarisation(PDP), Linear Polarisation Resistance(LPR), and Electrochemical Impedance Spectroscopy(EIS).

The electrochemical experiments during the first 24-hour exposure of AA2024-T3 to inhibitors exhibited that 2,5-Dimercapto-1,3,4-thiadiazole acts as a corrosion accelerator, while Na-Mercaptoacetate and Mercaptobenzimidazole showed the most inhibitive performance among the tested organic compounds. On monitoring their nature during 24 hours, it was observed that they show stable polarisation resistance values after 6 hours. Among the inorganics, Cerium compounds were seen to have better inhibitive properties than the Lithium compounds. Additionally, surface studies such as Fourier Transform Infrared Spectroscopy (FTIR) revealed the presence of thiol/mercaptan and carboxyl groups on samples exposed to Na-Mercaptoacetate. X-ray Photoelectron Spectroscopy (XPS) showed oxides of Cerium on samples exposed to Cerium Nitrate. Finally, the correlations between the inhibition efficiencies calculated from different electrochemical testing methods were illustrated using Pearson's correlation method.

NOMENCLATURE

Abbreviations

AA	Aluminium alloy	
ATR	Atenuated Total Reflection	
CCC	Chromate conversion coating	
EEC	Electrical equivalent circuit	
EIS	Electrochemical Impedance Spectroscopy	
emf	Electromotive force	V
$EPMA$	Electron Probe microanalysis	
$FTIR$	Fourier Transform Infrared Spectroscopy	
GP	Guinier-Preston zones	
$I.E$	Inhibitor efficiency	%
IMP	Intermetallic particles	
LPR	Linear Polarisation Resistance	
OCP	Open Circuit Potential	V
PDP	Potentiodynamic Polarisation	
$REACH$	Registration, Evaluation, Authorization and Restriction of Chemicals	
SCC	Stress Corrosion cracking	
SHE	Standard Hydrogen electrode	V
XPS	X-ray Photoelectron spectroscopy	

Mathematical notations

ω	Angular frequency	$\mathrm{rad\,s^{-1}}$
ϕ	Phase shift	$^\circ$
p	Pearsons correlation coefficient	
Z	Impedance	Ω

Symbols

α_a	Anodic charge transfer coefficient	
α_c	Cathodic charge transfer coefficient	
η	Efficiency	%
η_o	Overpotential	V
λ	Wavelength	m
ρ	Density	gm^{-3}
j^b_{corr}	corrosion current density without inhibitor	Am^{-2}
j^i_{corr}	corrosion current density with inhibitor	Am^{-2}
R^b_p	Polarisation resistance without inhibitor	Ω
R^i_p	Polarisation resistance with inhibitor	Ω
R_p	Polarisation resistance	Ω
a	Molar mass	$gmol^{-1}$
b_a	Anodic slope constant	$mVdecade^{-1}$
b_c	Cathodic slope constant	$mVdecade^{-1}$
E	Electrode potential	V
E_{app}	Applied potential	V
E_{corr}	Corrosion potential	A
E^o	Standard electrode potential	V
emf	Electromotive force	V
G	Gibbs free energy	$Jmol^{-1}$
i	Current	A
i_{corr}	corrosion current	A
i^0	Exchange current	A
j	Current density	Am^{-2}
j_{corr}	corrosion current density	Am^{-2}
k	Wavenumbers	m^{-1}
n	no of equivalents exchanged per mole	mol^{-1}

Q_r	Reaction quotient	
T	Absolute temperature	K
t	time	s
w	Mass of the metal corroded	g
z	number of electrons exchanged	

Universal constants

F	Faradays constant	$96\,500\,\mathrm{C\,mol^{-1}}$
R	Gas constant	$8.314\,\mathrm{J\,mol^{-1}\,K^{-1}}$

CONTENTS

LIST OF FIGURES

LIST OF TABLES

1

BACKGROUND

1.1. CORROSION BASICS

Corrosion in layman's terms can be explained as the deterioration of the material due to its reaction with the environment. The environment could be air, humidity, water (aqueous), acids, alkalies, industrial gases and chemicals, etc. By referring here to 'material', the emphasis is on metals in specific. Other materials might corrode too, nevertheless this report deals with corrosion of metals only, and especially aluminium alloy AA2024-T3 which will be referred at the later stages. D Jones in his book [20], rightly addresses corrosion as *Extractive Metallurgy*, due to the fact that this process returns the metal to its chemical compounds as they were originally present. Unlike other metals, noble elements such as Ag, Au, Pt, Pd usually do not corrode due to their nonreactive nature with environment [9, 20–24].

Corrosion pose wide range of concerns. Right from the direct human and safety concerns to economic costs involved in prevention, monitoring and study. Numerous drastic effects were recorded that were identified to the direct cause of corrosion. On 28th April, 1988, the cabin of an commercial aircraft (Aloha) in Hawaii suddenly disintegrated (Figure 1.1a) causing 1 fatality and 65 injuries. The collapse of Silver Bridge at Ohio (Figure 1.1b) on 15th of December, 1967, which caused 46 fatalities was later investigated and it was concluded that the underlying cause was stress and corrosion. The economic costs of corrosion in the United States were reported to be around 276 billion US$ annually. Around 3-5% of a country's Gross National Product is consumed by corrosion. The direct costs include cost of replacement, maintenance, designing corrosion resistant alloys, protection coatings, inhibitors etc [21].

Corrosion is an inevitable process. Its detrimental effects can only be minimized or prevented up to a certain extent. Some general prevention techniques can be implemented as follows [20, 25, 26]:

1. Design of corrosion resistant metals.
2. Design modification.

3. Use of coatings.
4. Anodisation.
5. Cathodic protection.
6. Use of inhibitors.
7. Surface modifications.

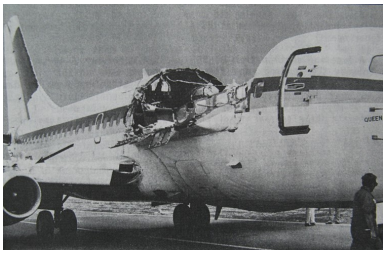

(a)

(b)

Figure 1.1: Impacts of corrosion. (a) Aloha airlines disintegration. (b) Silver Bridge collapse [1, 2]

The driving force behind corrosion to occur is the chemical nature of the metals. They can be chemically unstable in the environment that they are exposed to and thus, prefer to go into their stable form. The fact that corrosion involves exchange of electrons from the metal to the environment, it can be regarded as an electrochemical process [9, 21–24]. For corrosion to occur, there are 4 things that are necessary:

1. Anode
2. Cathode
3. Electrolyte
4. Metallic Path

An anode is the component where electrons are released. This is the place where oxidation takes place, thus increasing the metal's oxidation number. A dissolution of metal takes place which means that the metal ions are released into the electrolyte. One of the characteristic of this process is that the metal shifts to a higher valence state [9, 27, 28, 28]. A general anodic reaction, where 'z' number of electrons are released, is represented as:

$$M \rightarrow M^{z+} + ze^{-} \tag{1.1}$$

On the other contrary, cathode is the component that gets reduced, decreasing oxidation number. The electrons released by the anode are consumed by cathode. Thus, the characteristic of cathode is that metal shifts to a lower valence state. The cathodic

reaction is expressed as gaining of electrons. However, the reaction depends on the electrolyte and environmental conditions as well [9, 27, 28, 28]. The different cathodic reactions that could occur according to the environment in which corrosion occurs are listed below:

$$\text{Dissolved oxygen: } 2H_2O + O_2 + 4e^- \rightarrow 4OH^- \tag{1.2}$$

$$\text{Acid solution with limited oxygen: } 2H^+ + 2e^- \rightarrow H_2 \tag{1.3}$$

$$\text{Acid solution with oxygen: } 4H^+ + O_2 + 4e^- \rightarrow 2H_2O \tag{1.4}$$

$$\text{Metallic reaction: } M^{z+} + e^- \rightarrow M^{(z-1)+} \tag{1.5}$$

The quantification of the corrosion rate or kinetics is done by different approaches. One such method is by measuring of amount of material lost per unit of time and other, by measuring current generated from the oxidation of metal. Corrosion rate(r) is usually expressed in mm/year. Faraday' law gives a link between charge transfer and mass transfer of a metal. From this relation, the mass of metal(w) that is corroded can be represented in terms of corrosion current(i_{corr}), time(t), atomic mass(a), number of equivalents exchanged(n) and Faraday's constant(F) as shown in Equation 1.6 [21, 28].

$$w = \frac{i_{corr} \cdot t \cdot a}{n \cdot F} \tag{1.6}$$

The derivative of the above equation gives corrosion rate, which can be expressed based on particular corrosion current density (j_{corr}) and density of the material (ρ) is given by the relation in Equation 1.7 [21, 28]:

$$r = \frac{a \cdot j_{corr}}{n \cdot F \cdot \rho} \tag{1.7}$$

The thermodynamics of corrosion is governed by the Gibbs free energy of the metals and its interfaces. This Gibbs free energy is in itself a function of chemical potential and it is the driving force for any chemical reaction. The Nerst equation, as shown in Equation 1.8 gives the cell potential (E) for a general electrochemical reaction [9, 21, 25, 28].

$$E = E^\circ - \frac{2.303RT}{nF} \log Q_r \tag{1.8}$$

Where, E_o represents standard electrode potential, Q_r is the reaction quotient, which is the ratio of chemical activity coefficients of products to activity coefficient of reactants.

Corrosion can be classified into different forms on the basis of its mechanism and the characteristic of the deterioration. Broadly, corrosion is classified into 2 categories, uniform and localised. While steels, zinc, and other metals show a uniform corrosion, aluminium alloys including AA2024-T3 shows localised corrosion, i.e corrosion at specific locations. Conventionally, some of the types of corrosion are [14, 21, 25, 28]:

1. **Uniform Corrosion**: Most common form of corrosion. It uniformly distributes on the metal surface.
2. **Crevice Corrosion**: Corrosion occurring in confined spaces or crevices.
3. **Erosion Corrosion**: Corrosion due to action of abrasive particles, slurry or liquids flowing.
4. **Pitting Corrosion**: Localised corrosion causing pits or deep penetrations.
5. **Galvanic Corrosion**: Corrosion when two dissimilar metals are in contact with one another in presence of an electrolyte.
6. **Intergranular Corrosion**: Localised corrosion that occurs at grain boundaries or nearby regions.
7. **Stress Corrosion**: Corrosion due to applied stress.
8. **Micro-biologically Induced Corrosion**: Corrosion due to bacteria and fungi.

1.2. OVERVIEW OF ALUMINIUM ALLOYS

When it comes to the material selection for aerospace applications, aluminium alloys are the most preferred one. The use of aluminium alloys in aircraft manufacturing goes back in time to 1930's, mainly due to their excellent structural and light weight properties. Although, the recent developments in composite materials has found a way in their use for aerospace applications, the use of aluminium alloys still remains a viable choice for airframe components and fuselage skin. These alloys account for 60-80% of the total airframe weight. The major reasons that aluminium alloys are a good choice for aerospace applications are [14]:

1. Cost effectiveness.
2. Low density.
3. Excellent structural properties that include high specific strength and stiffness.
4. Excellent fabricability.
5. Good fatigue resistance and fracture toughness.
6. Variety of properties obtained when heat or mechanically treated.

The classification of aluminium alloys can be done according to the different alloying elements added to it [14, 29]. This can be seen in the Table 1.1. This report deals with a specific class of aluminium alloy known as AA2024-T3, which will be addressed in the later sections. Hence it is important to know the composition, typical properties, and microstructure of this particular alloy .

The typical composition of aluminium alloy can be seen in Table 1.2. It can be seen that the major alloying element in 2XXX series is copper. This particular class of aluminium alloys can be age hardened through thermal treatments. Copper forms high

Alloy series	*Main alloying element*	*Age hardenable?*
1000	Commercially pure Al (> 99% Al)	No
2000	Copper	Yes
3000	Manganese	No
4000	Silicon	Yes (if Magnesium present)
5000	Magnesium	No
6000	Magnesium and silicon	Yes
7000	Zinc	Yes
8000	Other (including lithium)	Yes

Table 1.1: Major alloying elements in aluminium alloys [14]

Alloy	*Cu*	*Mg*	*Mg*	*Zn*	*Cr(max)*	*Si(max)*	*Fe(max)*
2017	3.5 – 4.5	0.4 – 0.8	0.25	0.4 – 1.0	0.1	0.8	0.7
2018	3.5 – 4.5	0.45 – 0.9	0.25	0.2	0.1	0.9	1.0
2024	3.8 – 4.9	1.2 – 1.8	0.3	0.3 – 0.9	0.1	0.5	0.5
2025	3.9 – 5.0	0.05	0.3	0.4 – 1.2	0.1	1.0	1.0
2048	2.8 – 3.8	1.2 – 1.8	0.25	0.2 – 0.6		0.15	0.2
2117	2.2 – 3.0	0.2 – 0.5	0.25	0.2	0.1	0.8	0.7
2124	3.8 – 4.0	1.2 – 1.8	0.3	0.3 – 0.9	0.1	0.2	0.3

Table 1.2: Composition of Al2XXX series. [14]

strength precipitate when age hardened by heat treatments. The 2XXX alloys are majorly used in structural and semi structural components. High strength, toughness, and good fatigue resistance are the major characteristics of 2XXX series. These properties are achieved by the presence of alloying elements copper, magnesium and zinc, forming high strength precipitates through solid solution and precipitation hardening. Due to the precipitation, phases are formed that contain intermetallic particles (IMP) such as $CuAl_2$, Al_2CuMg, ZnAl. The role of manganese and chromium is to restrict grain growth by producing dispersoids. Grain size reduction is done by titanium, whereas silicon reduces the viscosity of aluminium, thus increasing its castability properties [14]. The mechanical properties of 2XXX aluminium alloys can be seen in the Table 1.3.

The age hardening process induces some major phases in the AA2024-T3. These phases can be stable and(or) metastable. To understand the phases present, the thermal treatment of this alloy and the typical phase diagram needs to be studied. The thermal treatment consists of 3 steps [3]:

1. Solution treatment.
2. Quenching.
3. Natural aging.

It is due to these steps that the alloy gets its designation 'T-3'. As seen from the Figure 1.2a, the first step includes heating the alloy up to specific temperatures, usually

Alloy	*Temper*	*Yield strength(MPa)*	*Tensile Strength(MPa)*	*Elongation(%)*
2017	T4	275	425	22
2018	T61	320	420	12
2024	T3	302	446	13.2
2024	T4	325	470	20
2024	T6	385	475	10
2024	T8	450	480	6
2025	T6	255	400	19
2048	T85	440	480	10
2117	T4	165	300	27
2124	T8	440	480	6

Table 1.3: Mechanical properties of Aluminium 2XXX series alloys [14]

solvus line of phase diagrams as shown as point 1 in Figure 1.2a. This allows the solute copper atoms to dissolve in the aluminium solution. Thus a homogeneous solid solution phase is formed, which is the 'α' phase. The second step is the quenching step, which is the cooling process. A quick cooling is done so that the solute atoms freeze and do not have enough time to diffuse out. Thus, an unstable supersaturated solid solution is formed. This phase is known as 'α_{ss}' phase. The third step is the natural aging process in which the solute particles diffuse out of the solution thereby forming finely dispersed precipitates. These phases include the 'θ' and 'S' phase. When naturally aged, they are in their most stable state, thus achieving the equilibrium of precipitates [3, 14].

The processes that are involved in phase transformations can be better explained with the help of GP (Guinier-Preston) zones. GP zones are fully coherent metastable precipitates. Every GP zones are replaced by more stable states. The processes take place in following manner:

$$\alpha_{ss} \rightarrow \text{GP zones} \rightarrow \text{Coherent } \theta'' \rightarrow \text{Semi-Coherent } \theta' \rightarrow \text{Incoherent } \theta \tag{1.9}$$

$$\alpha_{ss} \rightarrow \text{GP zones} \rightarrow \text{Coherent S''} \rightarrow \text{Incoherent } S' \rightarrow \text{High Mg content} \tag{1.10}$$

The GP zones mentioned above are a cluster of alloying element atoms. Usually, these GP zones are 1-2 atomic plane thick and form solute rich regions. This can be well understood from the Figure 1.2b. A microstructural study of AA2024-T3 through Electron Probe Microanalysis(EPMA) shows the different phases and IMP present [5–7, 30]. They are shown in Figure 1.3. The details of these phases and IMPs can be seen from the Table 1.4. It can be seen that are significant phases such as the 'θ' ($CuAl_2$) and 'S' (Al_2CuMg) phase, These are the most abundant phases in the alloy (around 2.7 % of alloy surface area and 60% of the surface area relative to other IMP) [6]. Along with it, due to the presence of alloying elements, other precipitates like β (Mg_2Si) can also be seen.

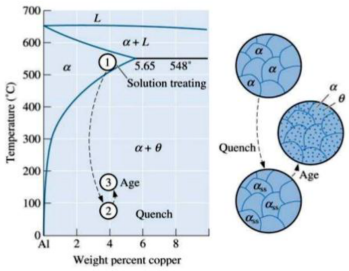

(a)

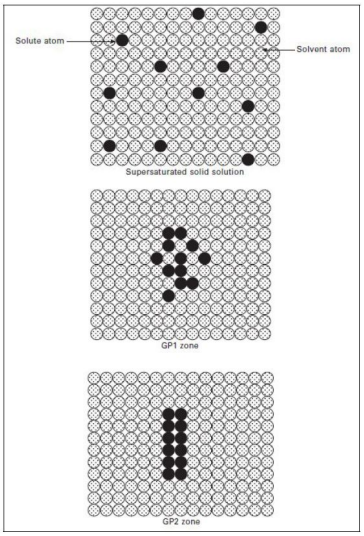

(b)

Figure 1.2: (a) Age hardening of AA2024-T3 and the phases present and (b) GP zones in AA2024-T3 [3, 4]

Table 1.4: Phase(s) composition in AA2024-T3 [5–7]

Phase	Color	Al	Cu	Mg	Mn	Fe	Si
Al matrix	Grey	96	2	1	0	0	0
$Al_{20}(Cu,Fe,Mn)_5Si\,(Al_8Fe_2Si)$	Yellow	77	5	0	5	10	4
$Al_2CuMg(S-phase)$	Mauve	61	20	15	0	0	0
$Al_2Cu(\theta\text{-phase})$	Orange	70	27	0	0	0	0
$Al_{10}(Cu,Mg)$	Green	90	7	2	0	0	0
$Al_3(Cu,Fe,Mn)$	Brown	73	11	0	4	10	1
Periphery	Cyan	81	12	4	0	0	0

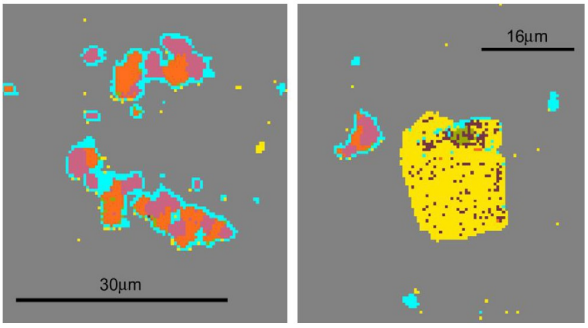

Figure 1.3: EPMA mapping of AA2024-T3, showing different IMP present. [5–7]

2

CORROSION AND CORROSION INHIBITION OF ALUMINIUM ALLOY

2.1. CORROSION OF AA2024-T3

2.1.1. CORROSION OVERVIEW OF AA2024-T3

While the alloys that have magnesium and silicon as their major alloying elements (AA 5XXX and 6XXX) show good corrosion resistance, the presence of IMP in AA2024-T3 makes it prone to corrosion. Based on the electrochemical background as discussed in chapter 1, the corrosion of aluminium can be seen as oxidation of aluminium to Al^{3+} as shown in Equation 2.1, and reduction of dissolved oxygen to form hydroxyl ions as shown in Equation 2.2. Hydrogen evolution is also possible at cathode if environment is acidic [5, 7]. The overall reaction can be seen in Equation 2.3. The anodic, cathodic and overall reaction that takes place are shown below:

$$Al \rightarrow Al^{3+} + 3e^{-} \tag{2.1}$$

$$2H_2O + O_{2(aq)} + 4e^{-} \rightarrow 4OH^{-} \tag{2.2}$$

$$4Al_{(s)} + 3O_{2(g)} + 6H_2O_{(l)} \rightarrow 4Al(OH)_{3(s)} \tag{2.3}$$

The corrosion resistance properties of AA2024-T3 is mainly due to the ability of the alloy to form protective oxide layer on it. Despite this resistance, it is highly susceptible to localised corrosion. Although a uniform corrosion of AA2024-T3 can also be seen, which happens when the alloy is subjected to strong acidic or alkaline solutions. In this case, the alloy is not able to form a protective oxide layer because the rate of dissolution of passive oxide layer is more than its formation rate [5, 11, 22]. When the electrolyte is trapped inside gaps between the alloy and any non metallic parts, it could lead to crevice corrosion. The thermal treatment induces some copper depleted regions at the grain boundary that corrode anodically, causing Intergranular corrosion (IGC). When

the alloy is subjected to tensile stresses in corrosive environment, it could show Stress Corrosion cracking(SCC) as well. Out of all the localised corrosion, the most common type of corrosion observed is the pitting corrosion which is discussed below [7, 9, 14].

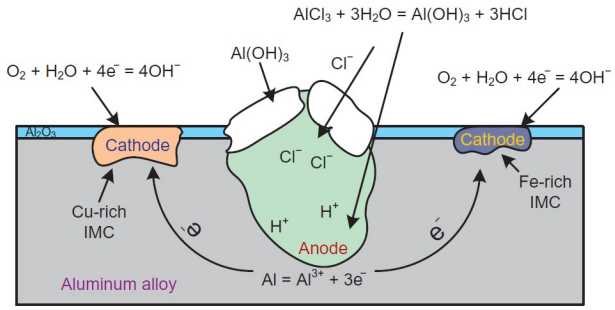

Figure 2.1: Pitting corrosion of Aluminium alloy in presence of NaCl [7]

2.1.2. PITTING OF AA2024-T3

Pitting involves shallow holes, undercuts, or penetrations that go deep into the material. Generally, pitting process can be categorized into 2 stages, pit initiation and pit propagation (or pit growth). The breakdown of passive film is mainly responsible for pit initiation. The breakdown of passive film occurs as a result of adsorption of chloride ions [6, 7]. When it comes to AA2024-T3, the pitting was studied in four stages. Initially, processes occur on the boundary of the passive film and the solution. This is where the adsorption of chloride ions takes place. Presence of micro-defects, voids, or irregularities in oxide layer are majorly responsible for this adsorption. Then, the chloride ions interacts with the passive layer. These two processes are related to the pit initiation stage. It is extremely difficult to monitor this stage. In the next stage, the development of pits takes place. Pitting is characterized by pitting potential (E_{pit}). Below this pitting potential, formation of metastable pits takes place, some of which can grow, and then repassivate, while others propagate further, leading to stable formation. Finally, in the fourth stage, when the E_{pit} is reached, formation of stable pits takes place. The transition from metastable pits to stable ones is characterised through a sharp current variation, as studied by Hughes A. et.al. [8]. At E_{pit}, current rapidly increases, as shown in Figure 2.2 and stable pits are formed. [31]. An overview of pit propagation and the electrochemical processes that occur can be seen in Figure 2.1. Anodic dissolution of aluminium and cathodic processes occurring at the phases that contain specific IMP are majorly responsible for pitting of this alloy. Hence, the role of IMP is a crucial step in understanding the corrosion phenomena at micro-level [7].

2.1.3. ROLE OF INTERMETALLIC PARTICLES IN CORROSION

The heterogeneous microstructure plays a crucial role in the corrosion of AA2024-T3. The different phases formed due to the various mechanical and heat treatments might increase the strength of alloy, but these IMP are responsible for the localised pitting and

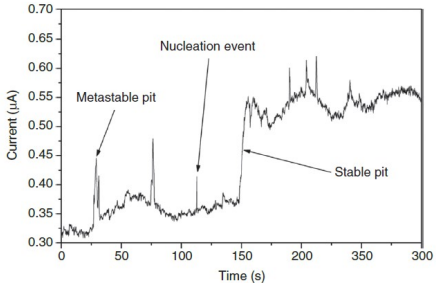

Figure 2.2: Current transition and processes involved in pit formation over time. [8]

exfoliation of the alloy. While a vast amount of literature suggests that the susceptibility of AA2024-T3 is due to the precipitates, Al-Cu, Al-Cu-Fe, and Al-Cu-Mn-Fe-Si that tend to be cathodic relative to the anodic aluminium matrix, it is still a topic of discussion so as to how exactly the 'S' phase contributes to the mechanism of corrosion. The active S phase selectively dissolves when exposed to aqueous solutions. The dissolution of active elements, such as aluminium and magnesium from the metallic phase leaves behind a porous copper rich phase. This copper rich phase when it attains nobility, act as cathodic sites enhancing oxygen reduction reactions. The formation of microgalvanic couplings between the Cu-rich IMP and the surrounding matrix gives rise to pit initiation [6, 8, 31–33].

A step by step identification of the activities that are involved eases the understanding of this complex process. This can be seen from the Figure 2.3. It was observed that when the alloy is subjected to Cl^- ions, it makes the oxide layer thin. Then, the dissolution of aluminium and magnesium from the IMP takes place, liberating hydrogen gas. The S phase becomes enriched in copper and act as cathodic site with respect to aluminium matrix. Copper is then redistributed to the surrounding solution, where it oxidises and electrochemically re-plates on the areas around IMP in the aluminium matrix. So, a porous copper layer which was formed earlier, and the copper re-deposition that took place around the IMP increases the cathodic area, thereby increasing cathodic reaction rate and driving the pit propagation to the surrounding area [6, 8, 16, 34–36].

2.2. PASSIVATION OF ALUMINIUM

For understanding the corrosion tendency of an electrochemical system, it is essential to know the passivation behaviour of the metal. Passivation of a metal is the process through which the alloy develops an oxide layer on it, thus making it 'passive'. It protects the alloy from the environment it is exposed to. The passivity and stability of aluminium can be visualised with pourbaix diagram. It is a plot of potential vs pH of a material that helps to visualise the corrosion regions, passive regions and immune regions [37, 38].

From the Pourbaix diagram of aluminium as shown in the Figure 2.4, three regions of aluminium can be seen. Aluminium is thermodynamically immune in the 'immunity region' as shown. However, when the potential increases from -1.7V, and if the pH is below 4, aluminium is susceptible to corrosion. This is the 'corrosion region' where

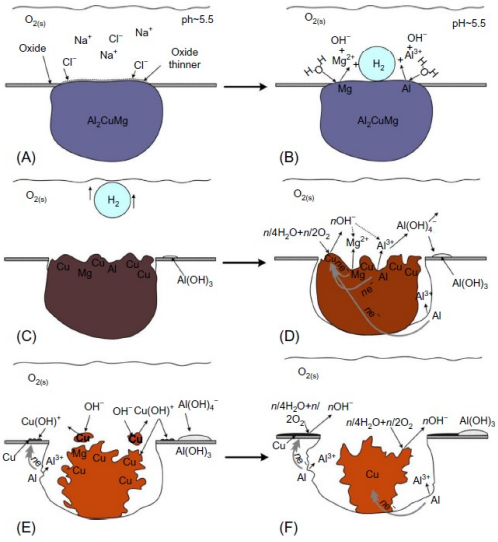

Figure 2.3: Corrosion mechanism of AA2024-T3 focusing on role of S phase in the pitting. [6, 7]

aluminium is stable as Al^{3+}. Another corrosion region is seen in alkaline range, that is in the pH range of 8.5 and above. Here, aluminium is stable as aluminate (AlO_2^-). The passivity of aluminium is achieved by $Al_2O_3.3H_2O$ layer and this is stable in the region of 4-8.5 pH. The regions between inclined 'a' and 'b' lines indicate region of water stability. The vertical lines showing -2, -4, -6 indicate the aluminium ion concentration of 10^{-2}, 10^{-4}, 10^{-6} respectively in gm ion/litre. Although the pourbaix diagram gives the valuable information on the thermodynamic stability, it does not give any information on the kinetics of corrosion. Temperature effects are also not considered. Moreover, this diagram does not take into consideration the effect of alloying elements on the thermodynamic stability [9, 37, 38].

2.3. CONSEQUENCES OF CORROSION OF AA2024-T3

The localised corrosion attack of AA2024-T3 has some direct consequences on the performance of these alloys in the long run. For instance, the propagation of pits into the material may result in chemical failure during its lifetime. When subjected to IGC, the challenges in monitoring it makes it difficult to study and if ignored, might lead to deterioration in mechanical properties [7].

Furthermore, AA2024-T3 possesses the problem of material embrittlement due to presence of hydrogen. The diffusion of hydrogen into the interior (hydrogen entrapment) of the metal through the hydrogen-metal interaction leads to the brittlement of the alloy. However, there is not a universally accepted phenomenon or mechanism that leads to the failure but a general feature that critical concentrations get build up at these potential sites that causes this failure. The lattice defects, grain boundaries, dislocations and vacancies provide trapping sites for the diffusion of hydrogen [8, 29, 30, 39].

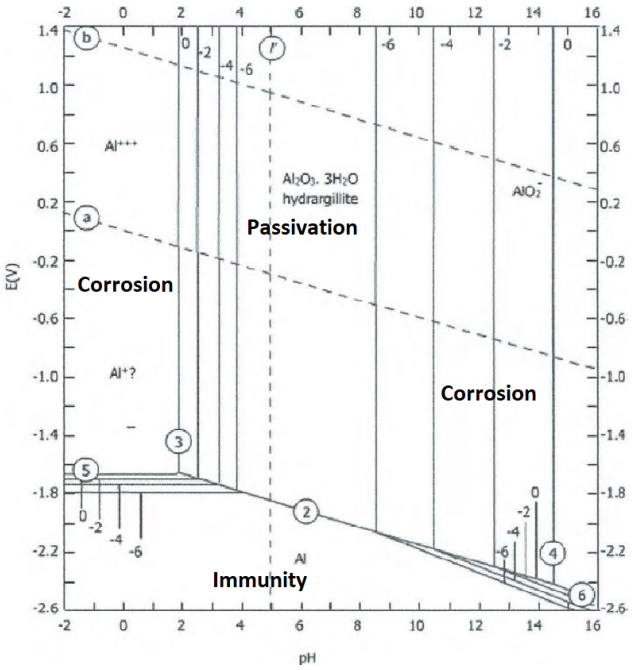

Figure 2.4: The potential-pH Pourbaix diagram for Al [9].

With these issues, it becomes necessary to develop protection strategies to combat the corrosion problem in AA2024-T3. These strategies include developing coatings that can be used as a barrier to protect the alloy from the corrosive environment to creating more 'active' type of protection by use of inhibitors, which is the focus of research.

2.4. CORROSION INHIBITION

The problem of corrosion in AA2024-T3 can be dealt by use of various corrosion inhibitors. An inhibitor is a chemical substance that when added to the corrosive environment, reduces the rate of corrosion. These chemical compounds significantly inhibit, prevent or reduce the corrosion rate even when they are used in minor amounts. The concentrations vary from a few ppm to as large as 15,000 ppm [26, 40]. Generally, inhibitors get adsorbed onto the metal surface, forming a protective layer that acts as a barrier and prevents the ingress of aggressive environment. The inhibitor could also potentially react with the environment, reducing its aggressive nature by forming a complex product [13]. The inhibitors can be classified based on their chemical nature, the mechanism of action, the mode of protection, or the environment in which it is used. This can be seen in the Figure 2.5 below.

According to the mechanism in which inhibition takes place, they can be classified as anodic, cathodic and oxygen scavenger. Anodic inhibitors are those that decrease the anodic polarisation behaviour. The corrosion potential is moved to the cathodic direction.

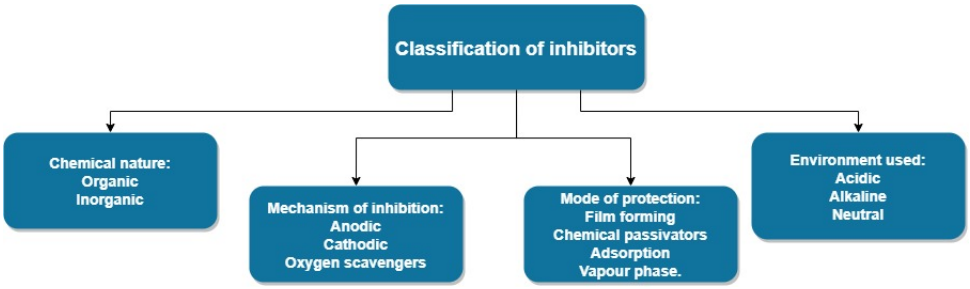

Figure 2.5: Classification of inhibitors.

These are also known as passivating inhibitors. They build a thin protective layer and increase the potential thus retarding the corrosion process. On the other hand, cathodic inhibitors are those which slow down the reduction reaction rate. These inhibitors shift the potential to more anodic direction. The potential shifts can be understood from the Figure 2.6 below. Oxygen scavengers are the type of inhibitors that remove the oxygen from the corrosive environment. This is achieved by reaction with oxygen and formation of complexes with it, thereby retarding corrosion process. While literature does suggest them to include in the cathodic type, but the difference in mechanism tends to recognise them separately. Another noteworthy type of inhibitors are the mixed type, wherein they retard both, the anodic dissolution and cathodic activities simultaneously. [9, 26, 41].

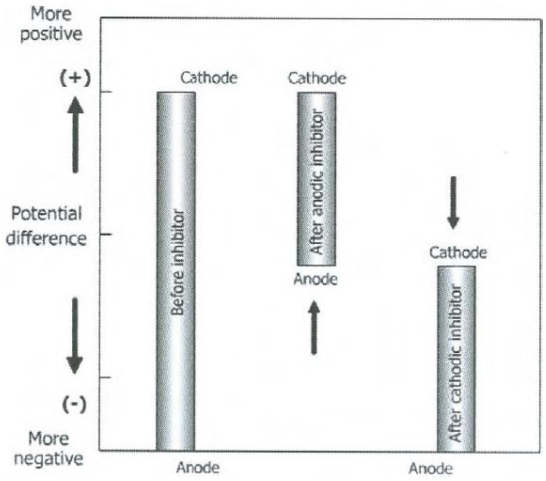

Figure 2.6: Effect of anodic and cathodic inhibitor on the potential [9]

The classification based on chemical nature of the compounds is pretty straightforward. Inorganic inhibitors could be chromates, phosphates, sulphates, vandates, lithium rare earth such as cerium compounds. Organic inhibitors are compounds that contain carbon-hydrogen as long chains and other functional groups attached to them.

They could be amines, mercaptans, azole derivatives, esters, nitro compounds etc. These are usually film forming and gets chemisorbed onto the surface [9, 26, 41].

The oxides of some compounds have been reported to inhibit in acidic environment. These are arsenic, antimony, tin, manganese and other heavy metal ions. Also, compounds containing oxygen, nitro and sulphur groups can be identified to inhibit in acidic environments. On the other hand, compounds such as phenols, ketons, etc are used in basic or alkaline environments [26].

2.4.1. USE OF CHROMATES AS INHIBITORS

The use of chromate compounds can be seen in variety of industrial applications. For instance, they are used as strengthening agents in steels, or fabricating oil tubing, automobile and ceramics applications. One of the important application of chromium is producing alloys that are highly resistant to corrosion and oxidation. Chromium exists in 2 oxidation states, +6 and +3 [42]. These hexavalent and trivalent chromium have found a way to be used as a corrosion inhibitors as well. For AA2024-T3, chromate compounds were found to be the most effective inhibitors. The electronic properties of these 'oxo' (Cr=O group) compounds make them a suitable choice for inhibition of aluminium alloys. The hexavalent chromium has a tetragonal structure and dissolve as stable complexes in water and transports to the surface and adsorb on it. Chromates are contained in deoxidisers, conversion coatings, sealants and paints, whereas the trivalent oxo-compound has a octahedral structure and is very stable and forms kinetically inert oxides [10]. One of the feature of these Chromate Conversion Coatings(CCC) is the self healing property wherein the diffusion and migration of these Cr^{6+} and adsorbing onto the Aluminium hydroxide layer through electrostatic or covalent binding. [43, 44]. The inhibition through CCC was observed in 3 stages, the release of Cr^{6+} species, inhibition of cathodic reactions, and attack at the active sites [45]. As seen in the Figure 2.7 below, chromate inhibitors can be incorporated into different scenarios, such as in aqueous solutions, in encapsulations to provide a self healing effect when defect occurs, or in conversion coatings.

Literature suggests vast advantages of using chromium compounds as inhibitors. These can be listed below[10, 43, 44, 46]:

1. Chromates can be used as both, anodic and cathodic inhibitors, thereby restricting metal dissolution and reduction reactions simultaneously.
2. Used in wide range of pH.
3. The chromium oxide layer formed is the best known for its inhibition properties due to its insolubility in aqueous environments.
4. The chromium oxide film adheres perfectly to the metal surfaces.
5. Durable and cost effective.

2.4.2. THE CHROMATE CONCERN

Although the chromium compounds have been observed as the best candidate as inhibitors for AA2024-T3, they are restricted to use for their toxic nature. Hexavalent chromium

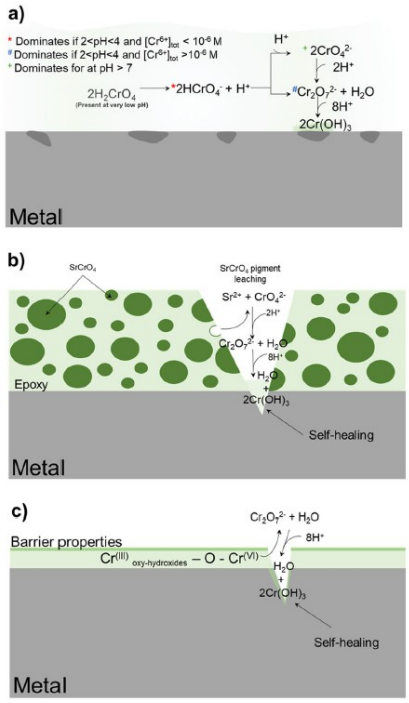

Figure 2.7: Scenarios in which chromium as inhibitors can be used: a. In aqueous solution. b. As self healing agents, and c. Chromate conversion coating [10]

.

was found to be carcinogenic in nature. The exposure to hexavalent chromium induced health damages. They were studied to be irritant to skin, nose throat, and eyes. People who were highly exposed to chromate compounds were seen to have higher rate of lung and nasal cancers than normal. Inhaling this would induce serious damage on nasal system and the ingestion would cause liver and kidney damage and genetic problems [10, 43–47]

Not only health problems, but use of chromates also raises some environmental concerns as it is expensive to handle and difficult to dispose. Unites States recognises 'hazardous waste' and observed that it primarily contains Chromium as the contaminant. The contamination of soil and water by chromates was seen to induce genetic toxicity on botanic and aquatic life [10, 43–47].

2.5. ALTERNATE COMPOUNDS USED AS INHIBITORS

Due to the concerns that chromium raises, as discussed in the earlier section, there has been regulations to restrict their use. Registration, Evaluation, Authorization and Restriction of Chemicals (REACH), which is an EU legislation, focuses on identifying and managing the risks associated to the use of these dangerous substances [10]. This comes down to recognising our research aim associated to this problem. To identify less (or

non) toxic compounds that can be used as inhibitors for AA2024-T3 and to test their performance.

For the past few decades, the restriction on the use of chromates has driven the scientific community to look for alternatives. Some of the compounds were tested for their inhibitive nature through electrochemical and surface analysis techniques. These are presented below:

To assess the inhibitive effects of Benzotriazole and Cerium Chloride, both, individually and combined on AA2024-T3 exposed to 0.05M NaCl, EIS measurements were carried out by Coelho E.B. et.al. [36]. The data depicted high impedance values of the protective layer which showed the formation of Cu-Benzatriazole as a protective film. As in the case of Cerium Chloride, the inhibitive film thickness was seen to increase over time, but the resistance of this film was decreasing, proposing a defective film due to the cerium deposits. Also, by increasing the inhibitor concentration, the corrosion resistance properties seemed to increase only in the initial time after immersion.

Lithium Carbonate as an inhibitor for AA2024-T3 was tested for its time dependency by Meeusen M et.al. [48] through EIS. An Odd random phase EIS was used to study this behaviour. This technique uses multi-sine signal to excite the system over the frequency range. The advantages of using this is it decreases the standard deviation as the number of samples taken are less than conventional EIS. The authors tested the stability of the organic coating with and without lithium leaching inhibitor for 12 hours. By analysing the data through noise curves with a combination of non stationarity and non linearity, they found out that this unstable behaviour is related to the electrochemical processes that occur in the oxide layer when exposed without inhibitor and porous layer when exposed to lithium inhibitor.

The time dependent behaviour of different concentrations of Nd^{3+} as corrosion inhibitor for API X70 steel was done by Matrinez D.M et.al. [49], wherein, it was observed that for blank solution containing no inhibitor, oscillations in R_p were seen. This would then correspond to reorganisation of surface resistance due to metal dissolution. In the presence of inhibitor, during the first 10 hours, there was subsequent increase in polarisation resistance that remained constant as observed until the 100^{th} hour.

Imidazole , 1-methyl-benzimidazole and 2-mercapto-1methyl-benzimidazole as inhibitors for copper substrate were tested for their time dependent behaviour by Taheri P. et.al. [15] using LPR. Here, 2-mercapto-1-methyl-benzimidazole was found out to be the best of the three, showing a gradual increase and stability of R_p values over time, whereas, 1-methyl-benzimidazole showed decent resistance at start, but a gradual decrease in the first few hours. Imidazole on the other hand, showed higher resistance than the blank samples, but only for the first 20 hours. After that, it exhibited lower values than blank solution, thus acting as corrosion accelerators.

Although, there is literature available for the time dependent studies of corrosion inhibitors for steels [49] and copper as substrates [15] as seen above, there lacks a study of inhibitors that are used for Aluminum alloys and AA2024-T3 in specific. Hence, an LPR analysis, along with other electrochemical methods described above are necessary for the studying the time dependent behaviour.

Yasakau K. et.al. [6], studied the inhibition of AA2024-T3 through Cerium Nitrate and Lanthanium Nitrate compounds in 0.05 M NaCl by PDP tests with -200mV in the

anodic direction and 250mV in cathodic direction. They observed that two breakdown potentials are visible from the anodic branch of the curves and related them to the breakdown of S phase and the other corresponding to the start of intergranular corrosion. A continuous shift in polarisation curves after 10, 60, and 120 minutes of immersion also indicated that the inhibition is taking place. This decrease in the cathodic and anodic current is caused by inhibition through formation of Cerium hydroxide deposits on to the S phase intermettalic. From a brief comparison of the inhibition effect from Ce and La compounds, it was concluded that La shows a similar behaviour as Ce, but the effect of La was much less than that of Ce. Unlike Ce, the inhibiting effect of La was seen immediately after 10 minutes and stayed constant over 2 hours demonstrating a faster kinetics [6].

To study the inhibition of Cerium Chloride and Prasedymium Chloride (individually and when combined with Mercaptoactetate), PDP experiments were done by Catubig R. et.al. [50], wherein, potential scans were done from -300mV to 500mV with respect to OCP at a scan rate of 0.167mV/s. The authors observed that E_{corr} values were shifted to more cathodic potentials indicating that the compounds were cathodic inhibitors. A significant decrease in cathodic current densities also showed that they were cathodic in nature. Cerium Mercaptoacetate was seen to be the most effective of all the cerium containing inhibitors with the decrease in current densities up to 2 orders of magnitude as compared to the uninhibited samples containing only NaCl [50].

The active protection properties of Lithium Carbonate, Benzatriazole and 2Mercaptobenzothiazole were studied by Visser P. et.al. [17]. PDP experiments were performed after 24 hours of exposure by sweeping -200mV to 200mV (with respect to OCP) and a scan rate of 1mV/s. The samples that exposed to inhibitors were observed to have shifted in current densities, showing an inhibitive nature. The difference was seen to be in orders of magnitude as compared to the blank solution containing no inhibitor. The anodic polarisation curves showed a shift in pitting potential to more noble values. A comparison of passive ranges showed that 2-Mercaptobenzothiazole has the largest anodic passive range as compared to the other inhibitors. A decrease in i_{corr}, shift in E_{corr} and E_{pit} and change in passive ranges showed that all the inhibitors were both anodic and cathodic type (mixed) and 2-Mercaptobenzothiazole was the most effective out of the three [17].

FTIR was used by Gobara M. et.al. in [51], to characterize 'collagen', which was used as additive to the typical silica sol-gel coatings that were used as inhibitors. They observed bands at wavenumbers that corresponded to CH_2 bond bend, COO- symmetrical stretch, CO stretch. Additionally, peaks were also observed that corresponded to stretching vibrations of carbonyl group, N-H group, and asymmetrical stretch of CH_2 group. Thus, they were able to identify and confirm that the compound they extracted was collagen.

Surface phenomenons and chemisorption studies were done by Fockaert L.I et al. [52], on pure magnesium substrate exposed to 4 different organic inhibitors containing carboxylic groups, 2,5-pyridinedicarboxylic acid, 3- methylsalicylic acid, sodium salicylate and fumaric acid (FA). An Attenuated Total Reflection (ATR) FTIR studies in parallel to electrochemical studies through EIS was done, thus following an in-situ approach. It was observed that inhibition takes place through formation of Mg oxide/hydroxide layer

and then chemisorption of carboxyl group of the inhibitor on this layers.

Kozlica D. et.al. [53] studied 2-mercaptobenzimidazole and octylphosphonic acid and their mixtures as corrosion inhibitors on Al. The presence and interaction between these organic compounds and pure aluminium was done through ATR-FTIR with/without addition of inhibitors for 24 hours. The authors proved that octylphosphonic acid was present on the substrate throughout all the mixtures and showed strong inhibition properties. Peaks were identified that corresponded to P-O, P=O, P-C functional groups, which was evident that octylphosphonic acid is adsorbed to the aluminium.

The performance of inhibitors and studies related to mechanism of inhibition is certainly important while choosing an inhibitor. But this is not enough when it comes to industrial application. When it comes to long term applications, the compatibility of inhibitor to the substrate and the environment in which it is becomes a crucial task to study [6, 7, 38, 54, 55]

The alloy could be subjected to various environments, including acidic, neutral and alkaline. Inhibitors effective in one media can/cannot be effective in other. The solubility of inhibitors in the environment also needs to be considered. When incorporated in a coating, the leaching of inhibitors is the first step towards protection. Hence, understanding the 'leachability' of inhibitors, i.e. how fast and effective it leaches from the coating, is a significant task. Also, when the inhibitor is able to from a passive layer, it should retain its properties even when the inhibitor concentration decreases. This 'irreversibility' properties of Benzotriazole, 2-mercaptobenzothiazole and Lithium Carbonate was studied by Visser P et.al. [17], and found out that although the former two organic inhibitors should excellent performance, they showed a reversible nature, i.e. the inhibition properties vanished once the concentration of these inhibitors was reduced. On the other hand, Lithium Carbonate showed fast leaching properties, was seen to be effective and had irreversible nature [6, 7, 38, 54, 55].

The corrosion inhibition of AA2024-T3 through Cerium Sulphate and Melamine was studied by Gobara M et. al.[56], wherein XPS was used to investigate the oxidation state in which Ce exists on the substrate. The occurrence of Ce^{3+} showed that Ce^{4+} reduces to Ce^{3+} in the corrosive environment. To support their findings, they conducted XPS on Cerium Sulphate powder, which showed only Ce^{4+} peak, thus, concluding that the Ce must have reduced when it is present with melamine in the corrosion inhibition process.

3

Research Overview

The main aim of this thesis is to select environmentally friendly compounds and investigate their inhibitive properties on AA2024-T3. On the basis of literature, the upcoming research will be focused on meeting some major objectives and sub-objectives.

3.1. Objectives

1. To compare the electrochemical properties of inhibitors that can be used for AA2024-T3 by an experimental approach.
2. To perform an initial screening of the inhibitors and recommend the most effective ones.
3. To check with the consistency of screening process from the different electrochemical methods which were used.

The sub-objectives that can be identified are:

1. To study the time dependent behaviour of these inhibitors through LPR
2. To support the above studies through FTIR and XPS.

3.2. Research Questions

To meet the above objectives, it is necessary to frame some research questions . Hence, a total of 4 research questions were framed out:

1. What is the influence of the selected corrosion inhibitors on the electrochemical properties of AA2024-T3?
2. How to screen inhibitors on the basis of their electrochemical properties?
3. How does the presence of inhibitor affect the surface of AA2024-T3?
4. What are the discrepancies that arise from using different electrochemical techniques for inhibitor studies?

3.3. RESEARCH APPROACH

The following research is more of a breath focused than depth. Although there could be studies involving investigating the mechanism of a particular inhibitor, this research will focus on screening of different inhibitors and a quantitative study.

A typical study of corrosion inhibitors includes an extensive literature research and then testing of some of them experimentally. A similar strategy was followed here as well. To answer the research questions and to achieve the research objectives, an experimental approach was the best choice. Although computational approach can be followed as well, which will be addressed in the future research work. Experiments are strategically chosen taking into account suitability and availability of the research material. All of the experiments were conducted at the Electrochemistry and surface analysis labs at the department of Materials Science and Engineering, TU Delft. All of the instruments described below were available at these above mentioned labs. The experiments and methodology is reported in the following section. The data as analysed from the experiments is presented in the appendix and raw data files can be provided if necessary.

4

EXPERIMENTS

4.1. MATERIAL PREPARATION.

4.1.1. SUBSTRATE PREPARATION.

Bare AA2024-T3 sheets were used as substrates. They were received from 'Kaizer Aluminium' of length 2500mm and 2mm thickness and had typical a composition as shown in the Table 4.1. Their mechanical properties are presented in Table 4.2

Table 4.1: Elemental composition of AA2024-T3 as received from Kaizer Aluminium.

Si	Fe	Cu	Mn	Mg	Cr	Zn	Ti	V	Other
0.08	0.19	4.6	0.56	1.3	0.01	0.11	0.02	0.01	0.05

Table 4.2: Mechanical properties of AA2024-T3 as received from Kaizer Aluminium

Alloy	Temper	Yield strength(MPa)	Tensile Strength(MPa)	Elongation(%)
2024	T3	309	466.5	20.75

The sheets were first cut into 20*20 mm dimensions by using Automatic shearing machine. The cut samples were then grind manually with Struers SIC 320grit size sanding paper to remove any bends and surface irregularities that could have raised from the shearing process. Then, multiple samples were taped on a sample holder for automatic polishing machine. Aluminium being a soft material, MD LARGO (300mm diameter) fine grinding disc provided by Struers was used. It was mounted on 'Struers ROTOPOL-31' magnetic disc fixation. A program was set for fine grinding and polishing on 'Struers ROTOFORCE-4' automatic polishing machine with the following commands: Force: 25N, RPM: 150, Time: 6 minutes, Water: OFF and selecting the appropriate mode from among MD LARGO, MD MOL and MD NAP accordingly. All the discs were cleaned

with detergent and dried with iso-propanol before every use. Once the program was set, the samples were mounted, and initially MD LARGO was used as grinding paper. A continuous stream of water was used as a lubricant during this step to remove the particles from the grinding process. Next, for polishing, MD MOL was used and a 3μ diamond paste was used. Then, a fine polishing with MD NAP was used with a 1μ diamond paste. The polished samples were removed, rinsed with water and then with iso-propanol and dried. The samples were then kept in 'EMAG-EMMI 30HC' ultrasonic cleaner at full ultrasound efficiency for 10-12 min to remove any particulates and finally cleaned and dried with iso-propanol. Having a good and same surface finish on all the samples is necessary for reliable electrochemical measurements. This is because even a slight scratch on the sample might lead to concentration of corrosive activity around the scratch and create significant errors in the electrochemical measurements. For this reason, all the samples were observed under optical microscope to ensure that there are no major scratches after sample preparation, especially on the central part that was going to be exposed for electrochemical measurements as shown in Figure 4.1.

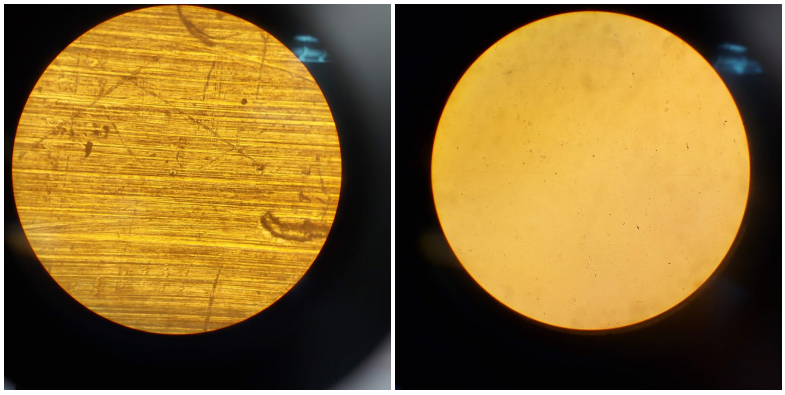

Figure 4.1: Samples observed under optical microscope before and after automatic grinding and polishing to ensure no scratches are retained.

4.1.2. INHIBITOR ELECTROLYTE PREPARATION.

For the inhibitor containing electrolyte preparation, the compounds were ordered and received in powder form. The sources are mentioned in the Table 4.3 for future use. Initially, concentrated stock solutions were made (with concentrations 0.1M or 0.01M according to convenience) and stored for future use. Finally, these stock solutions were diluted with demineralised water up to 1mM and 0.1mM concentrations with 0.1M NaCl added to it. For insoluble compounds, direct 1mM and 0.1mM solutions were made and kept stirring on heat for overnight or until completely dissolved. The solubility of compounds can be found out in the Table A.1 in the Appendix A

Table 4.3: Inhibitor compound specification.

Sr no.	Inhibitor compound	Nomenclature used	CAS number	Provided by
-	Basic salt	Blank salt	7647-14-5	J.T Baker
1	Lithium Carbonate	LCO	554-13-2	Sigma Aldrich
2	Lithium Nitrate	LN	7790-69-4	Alfa Aesar
3	Lithium Chloride	LCl	7447-418	Sigma Aldrich
4	Cerium Nitrate	CN	10294-41-4	Sigma Aldrich
5	Cerium Chloride	CCl	18618-55-8	Fluka Sigma Aldrich
6	Cerium Carbonate	CCO	54451-25-1	Alfa Aesar
7	Benzotriazole	BZT	95-14-7	Sigma Aldrich
8	2,5 DiMercapto 1,3,4 Thiadiazole	DMTD	1072-71-5	Sigma Aldrich
9	Sodium Acetate	NaAc	6131-904	Fluka ChemiKa
10	2-Mercaptobenzimidiazole	MBDA	583-39-1	Sigma Aldrich
11	2-Mercaptobenzoate	MBA	134-23-6	Thermo Fischer Scientific
12	Sodium Mercaptoacetate	NaMA	367-51-1	Sigma Aldrich

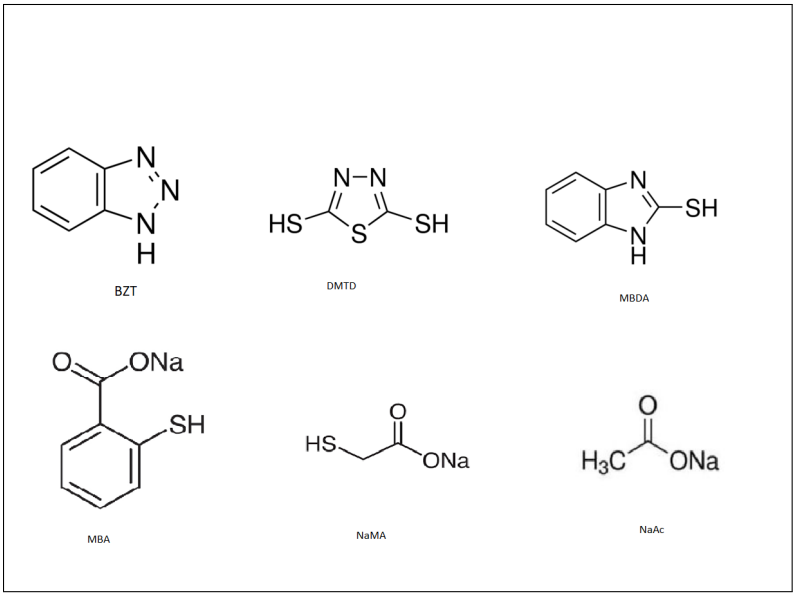

Figure 4.2: Structure of organic compounds.

4.2. ELECTROCHEMICAL ASSESSMENT.

A 3 electrode setup as shown in Figure 4.3 was used for all the electrochemical experiments. Flat cells were preferred over the conventional vertical red cells. This was to eliminate the case of inhibitors precipitating on the surface due to gravity. Additionally, they were easy to handle, and the amount of electrolyte containing inhibitor salt solution could be measured and kept constant(300mL). In the 3 electrode system, the working electrode was AA2024-T3 sample, the reference electrode was Ag/AgCl or the Saturated Calomel Electrode (SCE) in KCl solution, and the counter electrode was Platinum mesh electrode which was already incorporated in the flat cells. The area of the working electrode that was exposed to the (inhibitor) electrolyte was 0.785 cm^2. This setup was kept constant throughout all the electrochemical measurements. The cell setup was connected to the Biologic multi channel potentiostat and kept in a faraday cage to ensure reduction of background noise and vibrations.

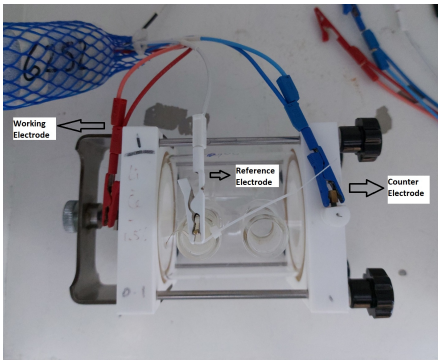

(a)

(b)

Figure 4.3: (a)Working electrode, counter electrode and reference electrode connected to the flat cell (b) Electrochemical cell setup placed in a faraday cage and connected to 'Biologic' potentiostat.

Once the cell was setup, a program was designed to test the electrochemical properties of inhibitors. As inhibition is a complex process, multiple electrochemical measurements are required to study the properties of inhibitor. This program consisted of LPR repeated for 9 times, followed by an EIS for 2 times, again, LPR for 128 times followed by EIS for 2 times. Finally, at the 24^{th} hour, Potentiodynamic polarisation test was done. This, being a destructive test was carried out at last. The experiment program can be seen in the (Flowchart) Figure 4.4. Each inhibitor with a particular concentration was tested with this program for 3 runs for reproducible results. If the results were not consistent, extra runs were performed. A detailed theoretical description of the techniques and the methods that were implemented is given below. The input parameters for all the electrochemical experiments is provided in the Appendix A.

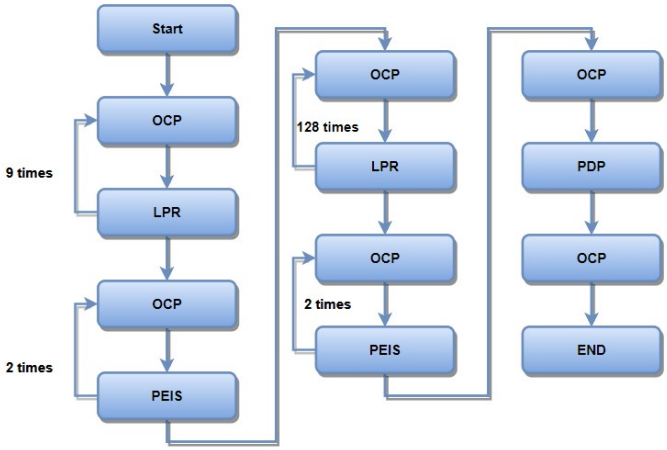

Figure 4.4: Program setup for the experiments.

4.2.1. OPEN CIRCUIT POTENTIAL(OCP)

THEORY

OCP is done for a particular amount of time so as to ensure thermodynamic equilibrium conditions are achieved and the system reaches to a stable potential. There is no application of any external potential or current. Once the rest potential is achieved, the samples can be polarised according to the experiments mentioned below. Thus, it is a preconditioning time used before every experiment.

METHOD

An OCP was done before every experiment. The rest time t_r was set to 10 minutes and data was recorded every 0.5 seconds within a potential range of -10V to 10V.

4.2.2. LINEAR POLARISATION RESISTANCE (LPR)

THEORY

LPR is a technique to measure the instantaneous polarisation resistance of a system. Unlike the potentiodynamic polarisation, this technique involves polarising the sample for 5-15mV anodically and cathodically with respect to OCP. From the Stern Geary equation as shown in Equation 4.11, it is known that the corrosion current is inversely proportional to the polarisation resistance. The Equation 4.8 and Equation 4.10 when reduced to simplest form gives the relation between overpotential and current as shown in Equation 4.1 and hence it is seen that current follows the overpotential (at some defined R_p). From the LPR, it is able to obtain the slope of these graphs (in the most linear parts) and this will be R_p as seen in Figure 4.5. With this value of R_p and appropriate values of tafel slopes, the corrosion current can also be calculated [15, 24].

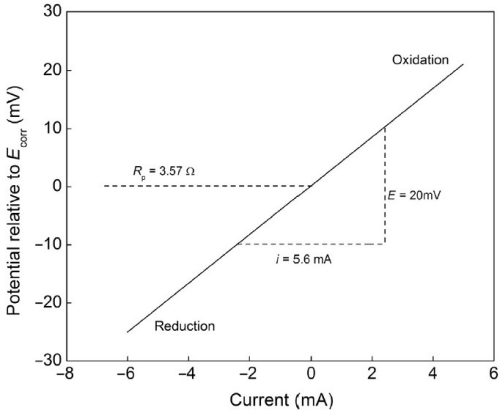

Figure 4.5: Measurement of Polarisation resistance [11].

$$\eta = R_p i \tag{4.1}$$

METHOD

A linear Polarisation Resistance was done initially for 9 times to monitor the time dependency of the inhibitors in the initial 10 minutes of immersion. ASTM-G59 standards were followed for this technique. The potential was sweeped between -10mV to 10mV with respect to OCP with a scan rate of 0.5mV/s.

4.2.3. ELECTROCHEMICAL IMPEDANCE SPECTROSCOPY (EIS)

THEORY

EIS is a useful tool to monitor and analyse the corrosion processes, which is an essential part in corrosion study. The oxide(or inhibitor) layer properties or systems that involve single or multiple coating, along with inhibition performance, and the passivity of the metal can be analysed through EIS. Hence, EIS is significant when it comes to studying the interface properties [11, 27, 36, 40, 57].

EIS studies the electrochemical system in terms of alternating current(AC) excitation at various frequencies. An input voltage or current is applied at various frequencies and accordingly, the output current or voltage is measured. The output signal can be phase shifted, or amplitude changed as shown in Figure 4.6 . This output is compared to the original input through impedance (Z) values as shown in Equation 4.4. For a general case of EIS, wherein potential is applied and current response is analysed, a general form of the input potential can be observed:

$$E_t = E_0 \sin(\omega t) \tag{4.2}$$

Where, E_t is the potential at time t, E_0 is the amplitude of the signal, and ω is the radial frequency.

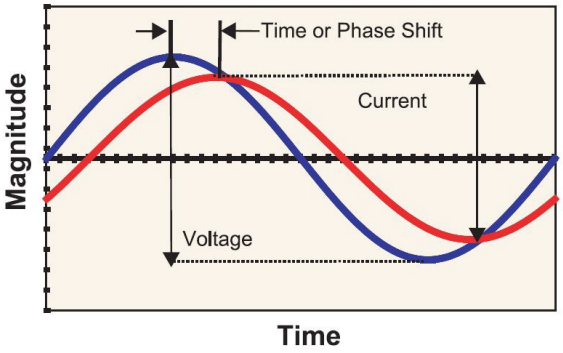

Figure 4.6: Representation of AC signals as sine wave with respect to time [5, 11].

$$I_t = I_0 \sin(\omega t + \phi) \tag{4.3}$$

Where, the response signal, I_t, is shifted in phase (ϕ) and has an amplitude, I_0.

$$Z = \frac{E_t}{I_t} = \frac{E_0 \sin(\omega t)}{I_0 \sin(\omega t + \phi)} = Z_0 \frac{\sin(\omega t)}{\sin(\omega t + \phi)} \tag{4.4}$$

Where, the impedance is expressed in terms of a magnitude, Z_0, and a phase shift, ϕ.

$$\exp(j\phi) = \cos\phi + j\sin\phi \tag{4.5}$$

$$Z(\omega) = \frac{E}{I} = Z_0 \exp(j\phi) = Z_0(\cos\phi + j\sin\phi) \tag{4.6}$$

The quantities can be expressed as a function of sines and cosines according to Euler's identity as shown in Equation 4.5.With this representation, the AC system can be mathematically written as a sum of imaginary and real components of impedance (with 'j' here, being the imaginary unit) as shown in Equation 4.6 [5, 11, 12]

The general principle of EIS is that an electrochemical system can be represented by a combination of resistors, capacitors and inductors. The output of EIS can be analysed by a typical Nyquist and Bode plots as shown in Figure 4.7 below. The Bode diagram is a plot of Impedance modulus over different frequencies whereas Nyquist plots represent the imaginary part of impedance and real part in a complex plane. Usually, a phase bode plot is also associated to the impedance bode plot that shows the phase angle variation through different frequencies. This is seen as the dotted plot in Bode plot below.

METHOD

A Potentiostatic Electrochemical Impedance Spectroscopy (PEIS) was done to study the impedance characteristics of the samples exposed to inhibitor along with other techniques. A single sine mode was used here. This means that system was excited by single frequency at a time. The system was scanned from an initial upper frequency(f_f) of

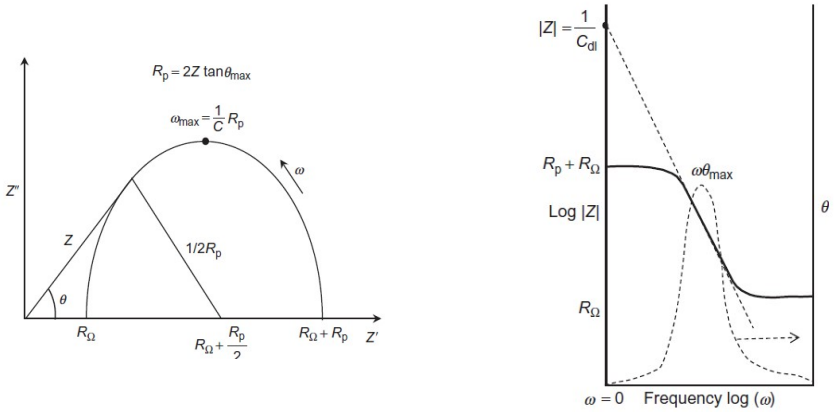

Figure 4.7: (a) A typical Nyquist plot of the corroding system (b) A typical Bode impedance and Bode phase plot(dotted) for corroding system [11, 12]

10KHz to a lower frequency(f_i) of 10mHz with 10 points per decade in logarithmic spacing.

4.2.4. POTENTIODYNAMIC POLARISATION (PDP)

THEORY

The term, 'potentio-dynamic' suggests that there is a change in potential. Thus, PDP tests involves varying the potential of a system and observing its behaviour [20, 27, 58]. This is the most widely used technique in corrosion testing as well as screening of inhibitors. The measurements provides values of i_{corr}, E_{corr}, tafel slope constants and different regions of the metal dissolution such as onset of pitting, active, passive regions. These parameters gives an idea about the cathodic and anodic characteristics about the system. Thus, the kinetics of the system as well as the mechanism is studied [48].

PDP is based on Butler-Volmer model and hence, the Butler-Volmer equation (as seen in Equation 4.7 below), becomes basis for understanding the theoretical background involved in these measurements [11].

$$i = i^{\circ}\left\{\exp\left(\frac{-\alpha_c F\eta}{RT}\right) - \exp\left(\frac{\alpha_a F\eta}{RT}\right)\right\} \tag{4.7}$$

Where, i is the current, i^0 is the exchange current, α is the (anodic and cathodic) charge transfer coefficient.

η is the overpotential and can be described as the difference between applied potential (E_{app}) and corrosion potential (E_{corr}) as in Equation 4.8.

$$\eta = E_{app} - E_{corr} \tag{4.8}$$

When the value of η becomes sufficiently large, i.e $\eta \to \infty$, the Butler Volmer equation becomes,

$$\eta = -\frac{RTi}{nFi^{\circ}} \tag{4.9}$$

By taking the derivative of this overpotential with respect to current, we get what is termed as Polarisation resistance (R_p) and is given by equation as shown in Equation 4.10.

$$R_p = \frac{RT}{nFi^{\circ}} \tag{4.10}$$

With this tafel approximation, the corrosion current (i_{corr})can be expressed as a inverse function of R_p and is represented by Equation 4.11.

$$i_{corr} = \frac{b_c b_a}{2.303\,(b_c + b_a)} \frac{1}{R_p} \tag{4.11}$$

Where, b_a and b_c denotes anodic and cathodic slope constants respectively. This is known as the Stearn-Geary equation.

The polarisation takes place with respect to OCP. It is usually 150-300mV above and below OCP and with a scan rate of 0.1-2 mV/s. Tafel extrapolation is used to analyse the PDP graphs. The intersection of the tangent lines from the linear region of anodic line and cathodic line represent the corrosion potential and corrosion current. At this point, rate of oxidation of metal is equal to the rate of reduction of H^+ ions. The effect of addition of addition of anodic and cathodic inhibitor can shift the PDP curves as shown in Figure 4.8.

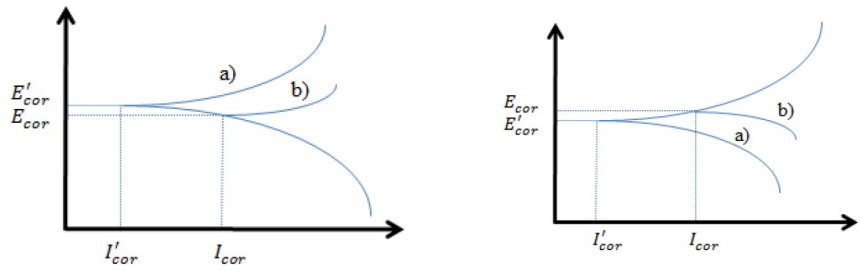

Figure 4.8: (a) Effect of addition of anodic inhibitor to the polarisation of system (b) Effect of addition of cathodic inhibitor to the polarisation of system. [9, 13]

METHOD

Potentiodynamic polarisation experiment was carried out on a 3 electrode system by polarising the sample from -250mV to 250mV wrt OCP with a scan rate of 0.5mV/s.

4.3. SURFACE ANALYSIS

With the electrochemical studies that are done to evaluate the performance and mechanism of the inhibitors, it was necessary to study the physio-chemical interaction between the metal and inhibitor compound to get a better understanding of the mechanism and relate to the electrochemical studies. Hence, surface analysis was done, in support of electrochemical measurements. Two of the surface analysis techniques which are discussed below were used for the research.

4.3.1. FOURIER TRANSFORM INFRARED SPECTROSCOPY (FTIR)

THEORY

One of the most common ways to obtain the substrate-inhibitor interaction through analysing(and identifying) the functional groups and their state, is through FTIR. It is a type of vibrational spectroscopy technique, wherein, a spectrum is obtained at various wavenumbers. It works on the principle that when a sample is exposed to infrared radiation, it absorbs some of the radiation, and transmits the rest. Different chemical structures produce different spectrum and a fingerprint analysis helps to identify the components present. The plot is usually an interferogram, which is the light intensity as function of frequencies that are summed up together. Then, a Fast Fourier transformation(FFT) is required to convert an interferogram to an infrared spectrum and hence the name, FTIR [52, 59, 60].

METHOD

EX-SITU FTIR

Figure 4.9: Ex-situ FTIR setup of AA2024-T3 exposed to 1mM NaMA placed on the 'Smart SAGA' accessory with exposed surface inverted.

Clean polished AA2024-T3 sample was immersed in demineralized water for 10 minutes to obtain a background spectrum. The sample was then removed, dried with purge of Nitrogen gas and then placed onto a 'Thermo Scientific Nicolet 6700' spectrometer. The spectrometer was initially cooled with sufficient liquid nitrogen. The spectrometer had a Mercury Cadmium Telluride (MCT) detector with KBr beamsplitter. For ex-situ FTIR measurements, a 'Smart SAGA' accessory was attached to the spectrometer. This

particular accessory had an integrated Germanium polarizer that enhanced the 'P' polarised light and eliminated the 'S' polarised component. The angle of incidence was kept fixed 80°with an exposed sample area of 5mm. Before collecting the background spectrum, the spectrometer was checked for 'Bench' and ensured it was within acceptable ranges. 'OMINIC' software was used to set the experiment program with 128 number of scans and a resolution of 8 (data spacing of 0.964cm^{-1}) because with this resolution, it was observed to produce resolvable peaks which were easy to notice and at the same time, didn't display noise. Transmittance spectra of the blank AA2024-T3 sample was recorded as background by placing the sample on the accessory with polished side kept upside down exposing to the IR beam as shown in the Figure 4.9. Then the sample was clean dried with nitrogen purge and immersed in a 1mM NaMA inhibitor containing solution for 1 hour. Finally, the spectra of inhibitor containing sample was recorded.

4.3.2. IN-SITU FTIR

For recording the in-situ measurements, the procedure was carried out in 3 steps:

First, pure Aluminium was deposited on the Attenuated total reflection (ATR) Germanium crystal by using the Physical Vapour Deposition(PVD) technique. A 'VCM 600-SP3' rack type vacuum evaporator was used for the deposition. Pure aluminium pieces were placed on the Tungsten boat filament. A holder was used to place this setup on the chamber and covered by a glass bell jar. Rough pump and turbo pumps were used to decrease the pressure in the glass chamber. After 3 hours, vacuum was achieved with a pressure reduction of $<5*10^{-6}$ bar. A program was set in the film setup menu, entering the material as aluminium and its parameters, density = 2.7 and Zratio= 1.8. The current was set to 100A and evaporation rate was monitored and kept constant with a value of of 0.1A/s. After a certain amount of time, a thin aluminium layer was seen to be deposited on the germanium crystal with an approx size of 20nm. After completion, the current and pressure knobs were turned off and the glass jar was removed and cleaned.

The second step included a cell setup for in-situ FTIR measurements. As shown in the Figure 4.10, the aluminium deposited ATR crystal was fixed onto a teflon bottom on one side. The lower side of the ATR crystal was kept fixed by using a crystal holder. A teflon electrolyte holder cup was used on the surface of teflon bottom that was exposed to the aluminium deposition. O-rings were used below the holder cup ensuring no leakage of electrolyte takes place. Screws were used to fix this assembly.

For the third and final step, the assembly was kept on to a 'VEEMAX III' ATR accessory as shown in Figure 4.11. The angle of incidence was kept constant at 65°. Similar to ex-situ measurements, this accessory was attached to a MCT IR spectrometer with liquid nitrogen cooling. Before collecting the background spectrum, the spectrometer was checked for 'Bench' and ensured it was within acceptable ranges. 'OMINIC' software was used to set the experiment program with 128 number of scans and a resolution of 8 (data spacing of 0.964cm^{-1}). Absorption spectra of the blank aluminium exposed to demineralised water was recorded as background. Once the background was collected, demineralised water was removed from the holder and 1mM NaMA solution was poured with a pipette. Absorption spectra were then noted for every 10 minutes up to 1 hour.

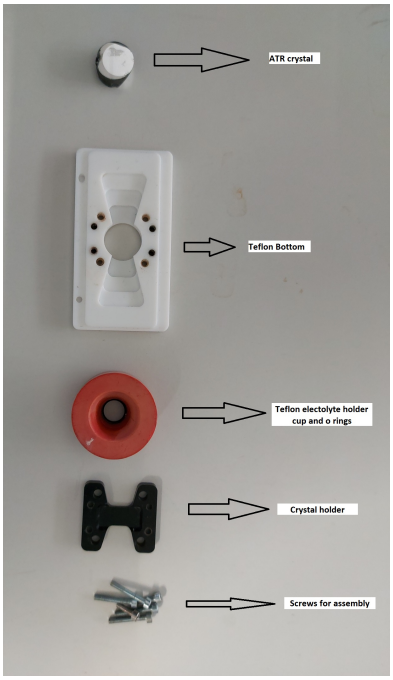

Figure 4.10: Assembly for in-situ FTIR

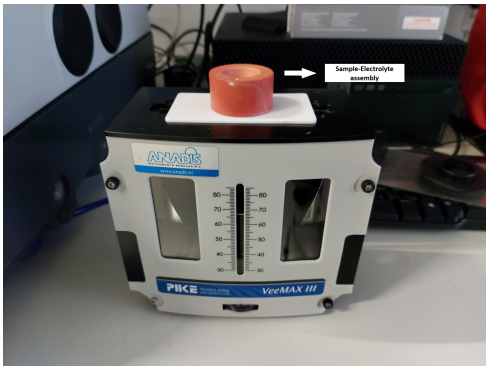

Figure 4.11: Sample-electrolyte assembly setup on the 'VEEMAX III' accessory for in-situ FTIR measurements.

4.3.3. X-RAY PHOTOELECTRON SPECTROSCOPY.

THEORY

Typically, inhibitors form a complex protective layer over the substrate, that is in the orders of few nanometers. The elemental composition of these thin films can be investigated by XPS. The outer 1-10nm of a solid surface can be detected for its chemical composition and the environment in which it is present. The basis of XPS is the photoelectric effect, which states that when a sample is irradiated by an X-ray, the energy of incident photons ejects an electron from the atom [61].

METHOD

X-ray photoelectron analysis was carried out using a PHI-TFA XPS spectrometer (Physical Electronic Inc.), equipped with an X-ray Mg-monochromatic source. The vacuum during XPS analysis was 10^{-9} mbar. The analysed area was 0.4 mm in diameter and the analysis depth was 3-5 nm. Narrow multiplex scans of the peaks were recorded with a step size 0.1 eV, at a take-off angles of 45°with respect to the sample surface. Low energy electron gun was used for surface charge neutralization XPS. Spectra were processed using Multipak v8.0 (Physical Electronics Inc.). The elemental composition was determined from the XPS survey spectra. High-energy resolution spectra of O 1s and C 1s and Al 2p, S 2p, Ce 3d, Ce 4d photoelectron peaks were curve-fitted.

5

RESULTS AND DISCUSSIONS

The study of inhibitors was divided into 4 sections:

Section 5.1 of this chapter deals with the comparison of electrochemical properties of the inhibitors. As discussed in the experimental section, this was done by LPR, EIS and PDP measurements. The systems were analysed in presence of inhibitors and it was compared with a system without inhibitors. This section gives a brief on the electrochemical properties of inhibitors and thus answers the first research question, 'What is the influence of the selected corrosion inhibitors on the electrochemical properties of AA2024-T3?'

Section 5.2 is a follow up of the previous section. A screening of the inhibitors can be seen here. Inhibitor efficiencies are presented for the selected inhibitors. From this screening, a study of properties of the 'best' inhibitor is done through surface analysis measurements FTIR and XPS. 'Which among the selected inhibitors perform the most effectively and could be recommended?'

Section 5.3 is a study of surface of AA2024-T3 samples when exposed to corrosion inhibitors. Considering the scope of thesis, only the best of the inhibitors from the screening process were investigated for their surface studies. This part of the chapter tries to answer the research question 'How does the presence of inhibitor affect the surface of AA2024-T3?'

Section 5.4 of this chapter discusses the discrepancies that arise from the different methods that were applied in the screening of inhibitors. The results from PDP, EIS and LPR are analysed and statistically analysed for the correlation among them. This tries to answer the research question,'What are the discrepancies that arise from using different electrochemical techniques for inhibitor evaluation?'

5.1. INFLUENCE OF CORROSION INHIBITORS ON THE CORROSION ACTIVITY

The PDP at 24th hour reflected some major information about the corrosion activity in the inhibitor containing samples. As discussed in subsection 4.2.4, corrosion activity is characterised by i_{corr}. When normalised through area, it can be considered as j_{corr}. The more is the corrosion activity, more is the value of j_{corr}. Hence, for a system in presence of an inhibitor, ideally j_{corr} should be relatively lower than the system that has no inhibitor.

The values of j_{corr} was found out from the PDP curves by Tafel approximation method. Data points from the anodic and cathodic branches was selected and a Tafel fit tool in E-C Lab software was implemented. Tangents were obtained for the best linear part from the curves. The degree of best fit was observed from the error associated to it. The intersection of anodic and cathodic branches is the j_{corr} point on the x-axis and E_{corr} point on the y-axis. The point of E_{pit} was also noticed as the point at which the anodic curve changes its behaviour and starts to pit.

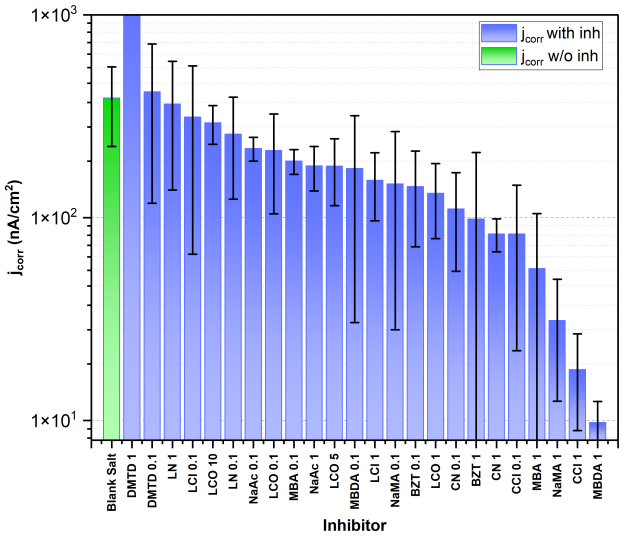

Figure 5.1: Corrosion current density of inhibited samples

As it can be seen from the Figure 5.1 above, the green column shows j_{corr} in absence of inhibitor, i.e. for a blank salt solution. It can be seen qualitatively and quantitatively that almost all of the inhibitor containing solution show less j_{corr} than the blank solution, except for DMTD 0.1 and DMTD 1. This indicates that DMTD acts as a corrosion accelerator instead of an inhibitor. When it comes to inorganic compounds, it can be seen that Cerium compounds can better decrease j_{corr} than Lithium compounds. In fact, CCl 0.1 and CCl 1 are able to reduce the j_{corr} up to one order of magnitude which shows that Cerium compounds are most effective, with CCl 1 being the best among those. CCl 0.1

and CCl 1 both exhibit less j_{corr} than CN 0.1 and CN 1, which suggests that the effect of chloride anion is favorable than nitrate anion. Corrosion current density can be directly linked to corrosion rate which indicates cerium compounds to exhibit lower corrosion rate than the lithium ones.

When it comes to organic compounds, it can be seen that MBDA 1 shows the least current density, which suggests excellent inhibitive properties. At the same time, MDBA along with, NaMA, BZT, MBA exhibit a large standard deviation in the values of j_{corr} with almost an order of magnitude of deviations from the mean values, which shows the have a lower reproducibility compared to inorganic compounds.

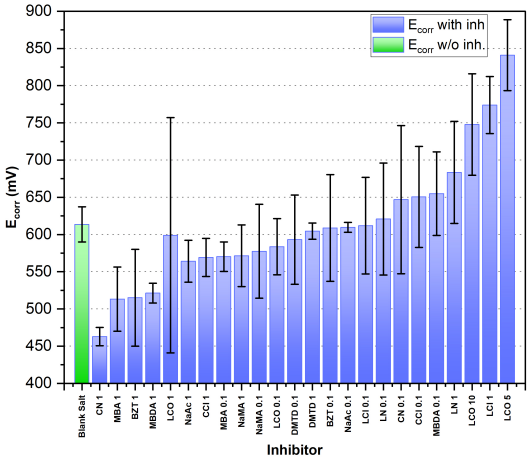

Figure 5.2: Corrosion potential of inhibited samples.

The corrosion potential of inhibitors can be seen in Figure 5.2. Note that these are the absolute values, E_{corr} is usually expressed as negative values. Hence a lowering of potential values here, means shifting to more anodic side as it an inverse graph, where the values indicate negative potentials. A limit of ±50mV (relative to uninhibited sample) was chosen as a criteria to understand whether an inhibitor works as a anodic type or cathodic type. CN 1, MBA 1, BZT 1, MBDA 1 seem to have a corrosion potential lower than the potential window of uninhibited sample. Hence, it is noted that they act as anodic inhibitors. On the other hand, LCO 1, LCO 5 and LCO 10 were seen to be acting as cathodic inhibitors. Others could act as mixed type, lowering both, anodic and cathodic reactions.

The pitting characteristics in the presence and absence of inhibitors can be seen from Figure 5.3. LCO 5, LCO 10, and DMTD 1 didn't show any onset of pitting. A possible reason could be that the pitting was already started when they were polarised or pitting potential value could be higher than the experimental range. Interestingly, it can be seen that most of the compounds exhibit the similar pitting potential, lying close to 500mV. This could suggest that the presence of inhibitor does not shift the pitting potential values. There might be a possibility that E_{pit} could be an intrinsic property of AA2024-T3

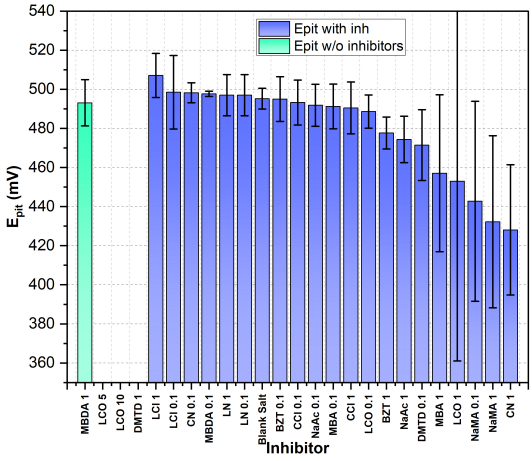

Figure 5.3: Pitting potential of inhibited samples.

5

and inhibitor does not play any role in the onset of pitting. The inhibitors could however, lower the E_{corr} values, thus increasing the passive potential range. A passive potential range is the difference between E_{corr} and E_{pit}. The passive ranges of the inhibitors can be seen from Figure 5.4. The passive range of LCl 0.1 was seen to be the largest, which exhibits good barrier properties. At the same time, CN 1 and MBDA 1, which were seen to have good inhibition properties, exhibited lower passive potential ranges.

The anodic and cathodic slope constant values of inhibitors is represented in Figure 5.5a and Figure 5.5b. Although the slope constant might not provide enough information on the surface properties or polarisation of sample, it gives an idea of how much overpotential is needed to increase the reaction kinetics by a factor of decade of current.

As it can be seen from the above results, PDP shows some information on the electrochemical parameters of inhibitors. However, it does not show how the parameters evolve with time. The time dependent behaviour of inhibitors can be obtained from LPR technique. The raw data obtained from the experiment was analysed for its R_p values. This was done by R_p fit tool from the EC lab software. From the large number of times that LPR was done, appropriate experiment data at specific hours, such as 0.5, 1, 2, 3, 6, 12, 18, and the 24^{th} hour was located and R_p values were obtained. These values of R_p were then plotted wrt time to get overview of R_p variation with time.

For LCO, increasing the concentration does not mean increasing in the inhibitive properties. Among the concentrations for LCO, LCO 1 shows evolving inhibitive properties. This can be noted from Figure 5.6. Until the 2^{th} hour, it was seen to be a continuous decrease in the R_p values, while it increased after 2^{nd} hour until 24 hour. The time dependent characteristics of lithium carbonate could be attributed to its inhibition mechanism. Lithium ions form complexes over the surface, by initially removing the protective aluminium oxide layer which is already present on the surface. This makes the system corrode for some time. An increase in the R_p values indicate the growth of this protec-

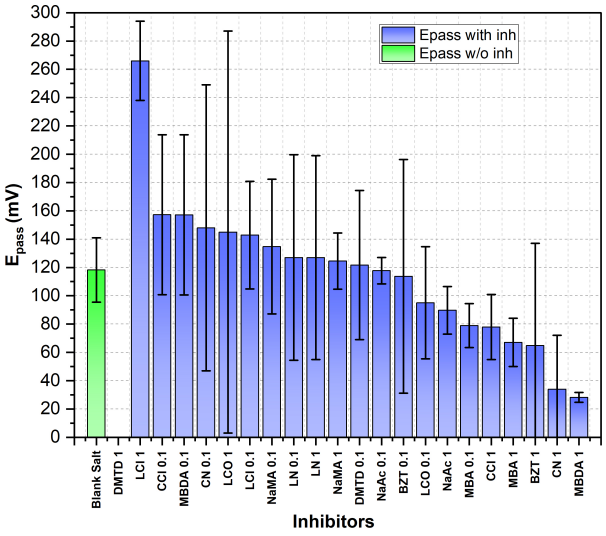

Figure 5.4: Passive potential range of inhibited samples.

tive layer formed by lithium ions. Past studies on Lithium inhibition indicate formation of multiple layers, dense porous and light over each other.

It can be seen from the Figure 5.7a that both the Cerium compounds CN 0.1 and CCl 0.1 were seen to have better R_p than the Lithium compounds throughout 24 hours with almost an order of magnitude difference between them. A comparatively stable trend is seen after 6 hours of exposure for CN0.1 and CCl 0.1, indicating some major inhibitive processes until 6^{th} hour. This can be well observed for CCl0.1 with an unstable characteristics until 6^{th} hour and lot of deviations in the R_p values throughout. On the other hand, Lithium compounds reflected low standard deviations, thus reflecting good reproducible results, as contrary to the literature, wherein it was seen that LCO do not exhibit reproducible results. But all of the Lithium compounds, LCO 0.1, LN0.1, LCl 0.1 were seen to have inhibitive nature until the 3^{rd} hour, but shows lower values of R_p than the blank solution after 3 hours of exposure. This trend suggests a strong time dependence on the performance of 0.1mM Lithium compounds.

The time dependence of R_p for 1mM Inorganic compounds can be seen in the Figure 5.7b. LN 1 and LCl 1 showed wavy characteristics again, exhibiting inhibitive and corroding properties throughout 24 hours thus, showing unstable behaviour. Overall, Cerium compounds were seen to have better trend than Lithium compounds. CCl 1 in specific, exhibited stable characteristics throughout 24 hours with less deviations in the R_p values.

For organic compounds, as seen from the Figure 5.8a, all of the compounds exhibited inhibitive properties, notice the R_p variation of all inhibitors is above the R_p line of blank salt solution line. NaMA 0.1 shows the highest R_p among all. Moreover, the variation in

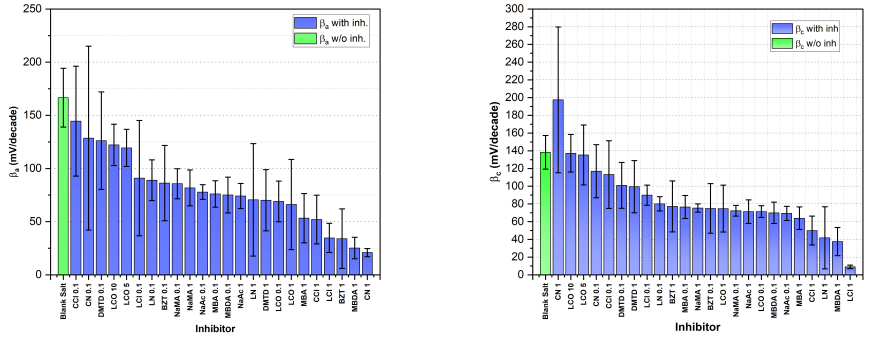

(a) (b)

Figure 5.5: (a) Anodic slope constant of inhibited samples (b) Cathodic slope constants of inhibited samples.

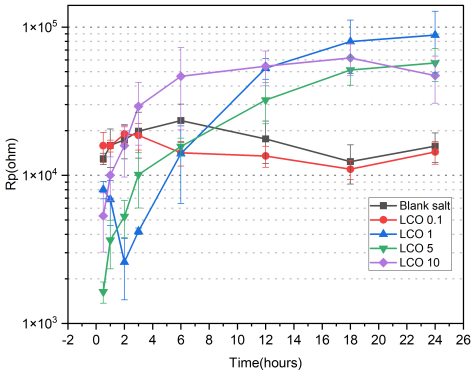

Figure 5.6: Time dependent characteristics of LCO of different concentrations.

the values throughout 24 hours is considerably small, which shows stable behaviour. It can be seen that DMTD 0.1 exhibits very good inhibitive properties in the initial stages, but drops down until 2nd hour, but manages to show stable characteristics after that. While most of the compounds show a decreasing trend in the initial hours and then a increasing trend until 24 hours, BZT 0.1 exhibits a continuous increase in the R_p values throughout 24 hours, indicating stable inhibitive properties. On the other hand, NaAc 0.1 and MBA 0.1 shows good inhibitive properties at the start, but a decreasing trend after 1st hour makes them poor inhibitors.

1mM organic compounds (refer Figure 5.8b) exhibit a distinctive behaviour. For most of the inhibitors, the R_p values were seen to be increased up to a considerable amount when the concentration was increased from 0.1mM to 1mM. MBDA 1 shows both stable, and good inhibitive properties throughout 24 hours. DMTD 1 although inhibiting at the start, shows a sudden drop in R_p values. This indicates a negative performance and

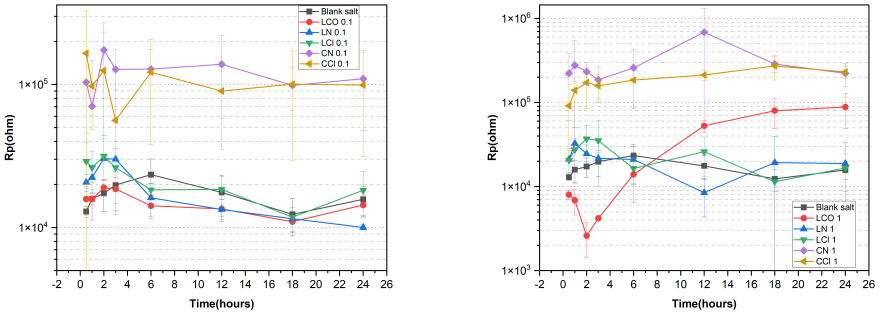

(a) (b)

Figure 5.7: Polarisation Resistance values of inorganic inhibitors of (a) 0.1mM concentration and (b) 1mM concentration plotted as a function of exposure time upto 24hours.

5

acting as a corrosion accelerator after 6 hours. NaMA 1 was seen to be the most effective, with some R_p variations in the start, which would indicate complex processes could be occurring while getting adsorbed on the surface.

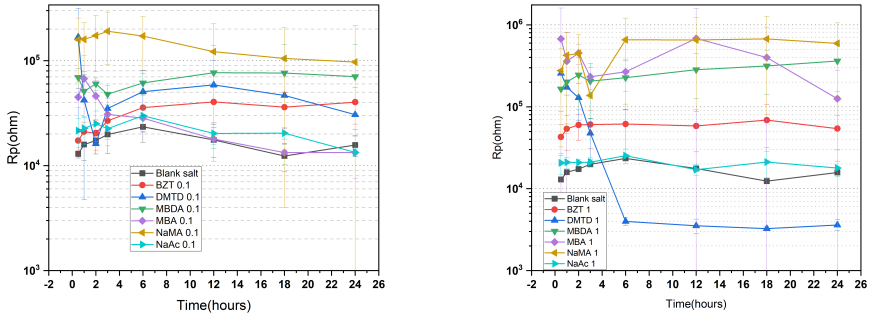

(a) (b)

Figure 5.8: Polarisation Resistance values of organic inhibitors of (a) 0.1mM concentration and (b) 1mM concentration plotted as a function of exposure time up to 24hours.

5.2. SCREENING OF INHIBITORS

A measure of how much a system with inhibitor can reduce the rate of corrosion can be expressed by inhibitor efficiency. It is not a absolute value, but rather a relative one. Typically, the rate of corrosion of a system when it is exposed to an inhibitor is compared to the system without inhibitor. IE is calculated by comparing the corrosion rates(CR) the formula as shown in Equation 5.1 below,

$$I.E = \frac{CR^b - CR^i}{CR^b} * 100\% \tag{5.1}$$

Where, superscript 'i' represents presence of inhibitor and 'b' represents blank solution in absence of inhibitor.

A total of 4 different methods were adopted to calculate IE as seen below:

PDP 24

As corrosion is an electrochemical process involving flow of electrons, the amount of current gives a measure of how much the system is corroding. Corrosion current or current density thus becomes a decisive factor to figure out the effectiveness of a system when it is exposed to inhibitor. Tafel extrapolations of PDP at the 24^{th} hour gives the corrosion current densities of different inhibitors as discussed in section 5.1. Hence with these values, the IE of each inhibitor was calculated according the Equation 5.2 below.

$$I.E = \frac{j^b_{corr} - j^i_{corr}}{j^b_{corr}} * 100 \tag{5.2}$$

EIS 24

EIS at the 24^{th} hour provided useful information about the Impedance characteristics of systems exposed to inhibitors. The value of R_p was noted down from the Bode plots as the the Impedance value at the lowest frequency. A relative measure of this R_p with respect to R_p of blank solution gave a measure of IE. The inhibition efficiency can be calculated from the formula as shown in Equation 5.3 below:

$$I.E = \frac{R^i_p - R^b_p}{R^i_p} * 100 \tag{5.3}$$

LPR 24

R_p values were fitted from the LPR which was done at 24^{th} hour. The same formula as shown in the Equation 5.3 was used to calculate IE.

EIS 2

Similar to EIS 24, the R_p values were noted down from the EIS at the 2^{nd} hour. IE was calculated as shown in Equation 5.3.

LPR AVG

Multiple LPR that were done throughout 24 hours were analysed for the inhibitor's time dependence characteristics. A trapezoidal numerical integration method for calculating the average R_p as seen in Equation 5.4 was implemented [15]. This R_p value was used to calculate the IE as shown in Equation 5.3

$$\langle R_p \rangle \approx \frac{1}{t_N - t_0} \sum_{k=1}^{N} \frac{R_p(t_{k-1}) + R_p(t_k)}{2} \Delta t_k, \tag{5.4}$$

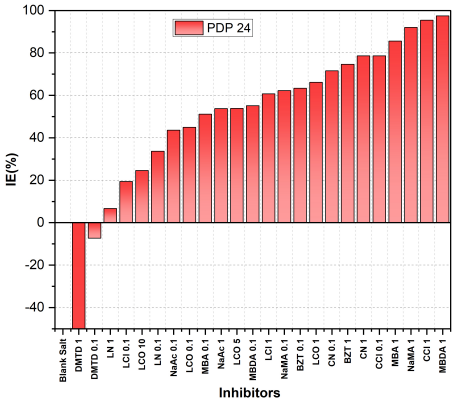

Figure 5.9: Inhibitor efficiencies as calculated from PDP 24.

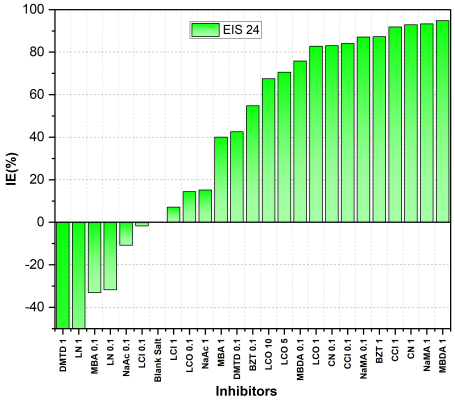

Figure 5.10: Inhibitor efficiencies as calculated from EIS 24.

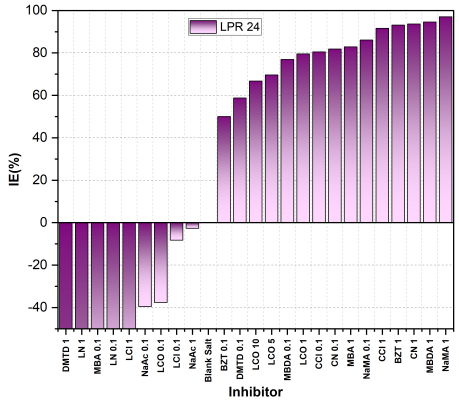

Figure 5.11: Inhibitor efficiencies as calculated from LPR 24.

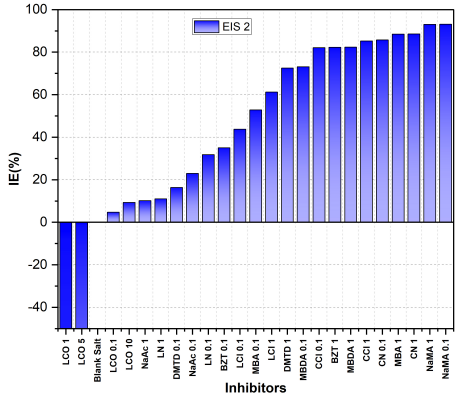

Figure 5.12: Inhibitor efficiencies as calculated from EIS 2.

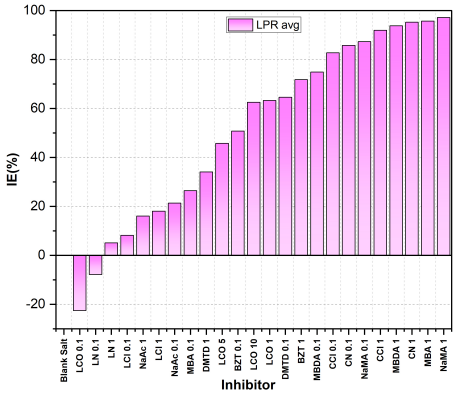

Figure 5.13: Inhibitor efficiency as calculated from LPR avg method

5

Figure 5.9 shows the efficiency of inhibitors as calculated from the PDP experiment at the 24th hour. As seen in section 5.1, in the The lowest j_{corr} was seen for MBDA 1 and NaMA 1, hence it is obvious that they show maximum efficiency. DMTD having more j_{corr} than the salt solution, shows a negative efficiency, indicating corrosion accelerating properties. Cerium compounds were seen to be more effective than Lithium compounds with CCl 1 having the highest efficiency.

More or less similar trend can be see in efficiencies from EIS 24 and LPR 24 methods, as seen in Figure 5.10 and Figure 5.11, with MBDA 1 and NaMA 1 having excellent efficiencies. Again DMTD 1 was observed to act as corrosion accelerator, and cerium compounds having better inhibitive properties than lithium compounds. However, LN 1, LN 0.1, MBA 0.1, NaAc 0.1, NaAc 1, LCO 0.1 and LCl 0.1 were seen to be corrosion accelerator. It is because at 24th hour, the R_p value decreases than the salt solution at that particular time.This can also be noticed from the time dependence studies above(Refer Figure 5.7a and Figure 5.7b).

Efficiencies as calculated from EIS 2 method however reflect contrasting numbers, as seen from the Figure 5.12. The ongoing corrosion processes and inhibition activities until 6th hour makes any measurement at 2nd hour prone to differences. CN1, NaMA 1 and NaMa 0.1 shows maximum efficiency due to its high R_p values after 2 hours. DMTD seems to be fairly inhibitive as well, with a positive efficiency, which is not the case as seen from its time dependent characteristics. Same applies with LCO 1 and LCO 5, which can be seen as highly corrosion accelerating, with negative efficiencies, but it is not the case as seen in the previous section.

LPR avg gives a good representation of efficiencies considering the time dependent characteristics of inhibitors. Again, NaMA 1, among the organics, and CN 1, among the inorganics, were seen to be highly effective (as seen from Figure 5.13).

A summary of all inhibitors and their characteristics is given in the Table 5.1 below.

Table 5.1: A summary of the screening process for all inhibitors

Sr no	Inhibitor	Nature	Comments
1	Lithium Carbonate (LCO)	Inorganic	Highly time dependent, fairly effective and stable after 6 hours
2	Lithium Nitrate (LN)	Inorganic	Unstable characteristics, poorly effective.
3	Lithium Chloride(LCl)	Inorganic	Unstable characteristics, poorly effective.
4	Cerium Carbonate (CCO)	Inorganic	Insoluble, cannot be used as inhibitor
5	Cerium Nitrate(CN)	Inorganic	Excellent effective, fairly stable behaviour
6	Cerium Chloride(CCl)	Inorganic	Excellent effective, stable at higher concentration.
7	Benzatriazole(BZT)	Organic	Moderately effective
8	2,5 DiMercapto 1,3,4 Thiadiazole(DMTD)	Organic	Ineffective
9	Sodium Acetate(NaAc)	Organic	Poorly effective
10	2-Mercaptobenzimidiazole(MBDA)	Organic	Excellent effective, stable for both concentrations.
11	2-Mercaptobenzoate(MBA)	Organic	Excellent effective with higher concentration, unstable behaviour
12	Sodium Mercaptoacetate(NaMA)	Organic	Excellent effective, stable after 6 hours.

5.3. SURFACE STUDIES

As it can be seen from the screening of inhibitors, NaMA 0.1 and NaMA 1 showed excellent characteristics even when calculating through different techniques. Hence, 1mM NaMA compound was chosen to analyse its effect on the surface properties of AA2024-T3 and its bonding characteristics with the substrate.

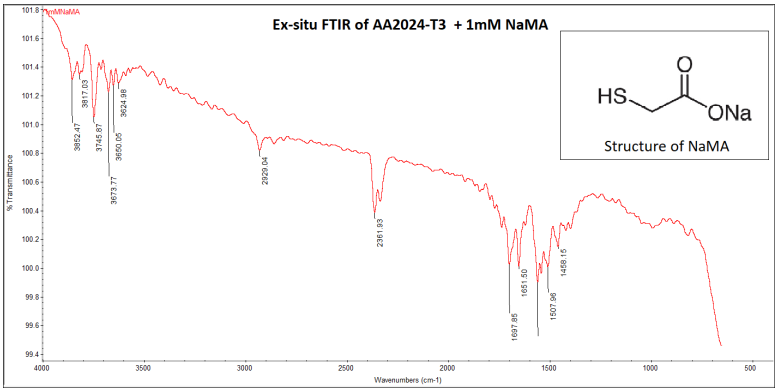

Figure 5.14: Transmission infrared spectra of AA2024-T3 exposed to 1mM NaMA for 1 hour.

The chemical structure of NaMA reveals that it has both, a thiol/mercaptan group (SH) and a carboxyl group (COO-). Now, whether any of those functional groups are adsorbed on to the AA2024-T3 surface was observed by ex-situ FTIR. The transmission spectra of AA2024-T3 exposed to 1mM NaMA for 1 hour can be seen in the Figure 5.14. The FTIR spectra can be divided into 2 regions, first, the region below 1500 cm^{-1} is the fingerprint region. This region is only an indicative of a functional group but does not give clear idea and careful analysis is required. On the other hand, the region from 1500cm^{-1} to 3000cm^{-1}gives a clear idea of the functional group present on the surface and hence called the functional group region. The region above 3000cm^{-1} is the one that typically relates to O-H stretching. It can be seen that after 1 hour of exposure of AA2024-T3 to 1mM NaMA there are sharp peaks at 1651 cm^{-1} and 1697 cm^{-1} wavenumbers which correspond to C=O symmetric and asymmetric stretching. However, no significant peaks relating to SH stretching or bending were observed. This means that the inhibitor does not get adsorbed through the thiol group on the aluminium substrate. However, it does not mean that it is not present on the surface. The presence of sulfur was observed through XPS data. Figure 5.15b shows the survey spectra of AA2024-T3 which was exposed to 1mM NaMA compared to a base sample which was not exposed to any inhibitor. Apart from the common peaks, additional Sulphur peaks at around 200eV are visible in the sample which was exposed to NaMA. Also, the atomic percentages are given, wherein Sulphur denotes to 0.5%,which is not so much in amount. This could be because of very low concentrations of NaMA. Interestingly, although with such less amounts, NaMA was seen to be an excellent inhibitor as discussed before.

A high resolution spectra of Sulfur was further analysed to see the chemical state it is present in. It is presented in Figure 5.17a. The data points from the experiment showed wavy characteristics and it was difficult to fit. After applying correction methods,

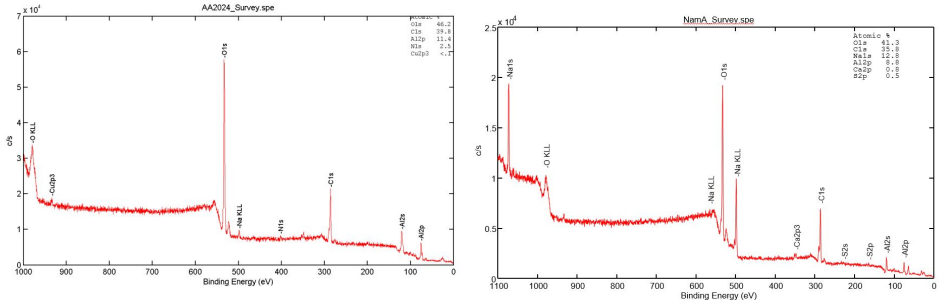

(a) (b)

Figure 5.15: (a) Survey spectra of AA2024-T3 (b) Survey spectra of AA2024-T3 exposed to 1mM Sodium mercaptoacetate

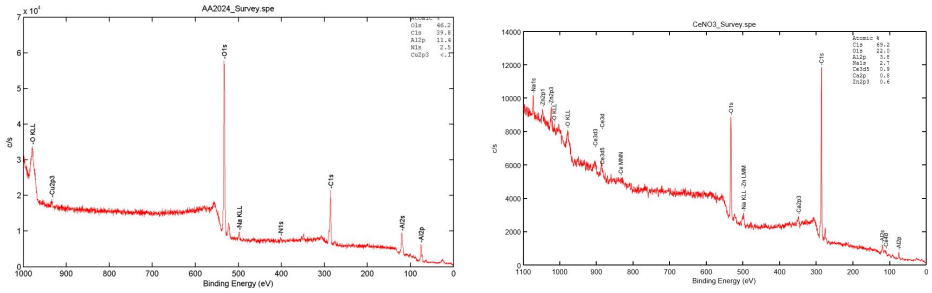

(a) (b)

Figure 5.16: (a) Survey spectra of AA2024-T3 (b) Survey spectra of AA2024-T3 exposed to 1mM Cerium Nitrate.

it was easy to identify the peaks. It can be seen that a strong peak exists at 163 eV with almost 80% area. This peak corresponds to mercapto group, which confirms that sulfur is present as mercaptan on the surface. Similarly, carbon peaks were fitted as seen from Figure 5.17b. A small peak at 289eV that corresponds to carboxyl group can be seen. Additional strong peak at 284eV can be seen which corresponds to the carbon chain (C-C) bonds present in NaMA.

The presence of cerium on AA2024-T3 was studied by XPS as well. Figure 5.16b shows the survey spectra of AA2024-T3 exposed to 1mM CN. Comparing it with the bare AA2024-T3 spectra as shown in Figure 5.16a, it can be seen that additional Cerium peaks at around 800eV-900eV are present. Again, the amount of Cerium is as small as 0.9% due to the lower concentrations of CN that was used. A high resolution spectra was analysed for these Cerium peaks to know the chemical state that they were in. Mainly, oxides of cerium can be seen in the high resolution spectra as shown in Figure 5.18a and Figure 5.18b. The sharp peaks fitted for Ce3d5 903eV and 885eV that contribute to around 40% and 36% of the area, shows Ce_2O_3 with +3 as the oxidation state. At the same time, cerium also showed to be present in +4 oxidation state with the presence of ceric oxides

as seen from the sharp peak at 115eV. However, the presence of Ce in +4 oxidation state suggests some oxidation takes place in the environment that can be studied later.

In-situ FTIR of pure aluminium exposed to 1mM NaMA was done in the first hour of immersion. Spectra was collected every 10 minutes until 1 hour to study the surface-inhibitor interaction in the first hour of immersion. As shown in the Figure 5.19, the lowermost blue spectra denotes the 1st measurement at 10 th minute and uppermost red spectra denotes the measurement at 60th minute, with intermediate spectra collected every 10 minutes. Similar to ex-situ measurements, the measurement can be analysed by studying the different regions, fingerprint region (for wavenumbers below 1500 cm^{-1}), functional group region (wavenumbers between 1500 cm^{-1} to 3000 cm^{-1}) and OH region (wavenumbers above 3000 cm^{-1}). In the functional group region, similar to the ex-situ measurements, there was no visible peak that could be assigned to thiol(SH) group. However, at around 2960 cm^{-1}, small peaks can be seen. This peaks correspond to O-H stretching in a carboxyl group. Additionally, a wavy characteristic that includes negative and positive peaks in the ranges 1500 cm^{-1} to 1700 cm^{-1} indicate C=O carboxyl group. A strong peak at 1630 cm^{-1} is visible. This peak corresponds to C=C asymetric and symmetric stretching, but since NaMA does not have any C=C alkene group, it can be assigned to N-H group. The presence of nitrogen is unknown, but it could be originating from the nitrogen purge that was used to clean the sample. In the fingerprint region, a strong peak at around 990 cm^{-1}is seen, which can be assigned to Al-OH denoting surface hydroxylation due to the immersion in demi-water. Thus, both, the ex-situ and in-situ measurements confirm the adsorption of NaMA to aluminium through the carboxyl group.

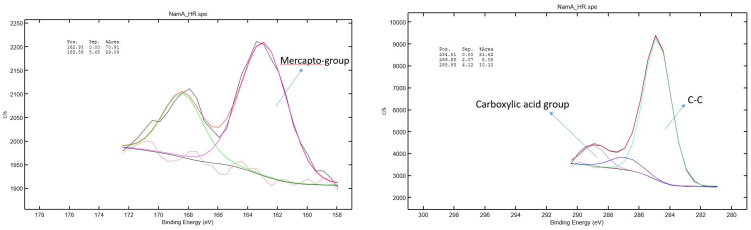

(a) (b)

Figure 5.17: High resolution spectra of (a)Sulfur and (b)Carbon for sample exposed to 1mM NaMA.

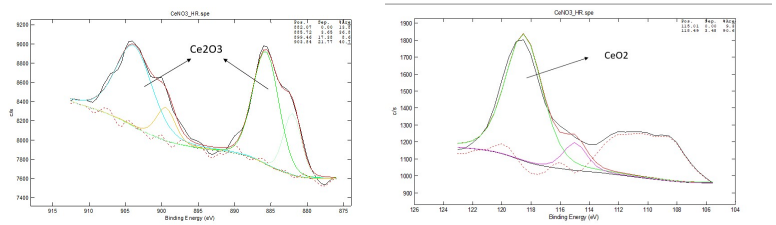

(a) (b)

Figure 5.18: High resolution spectra of (a)Ce 3d5 (b)Ce 4d5 of sample that was exposed to 1mM CN.

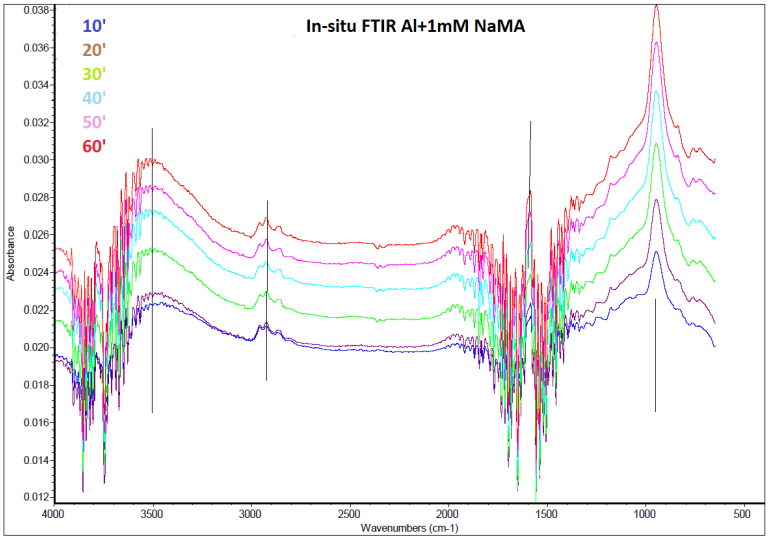

Figure 5.19: In-situ FTIR of pure aluminium exposed to 1mM NaMA. Spectra was collected every 10 minutes until 1 hour as shown.

5.4. COMPARISON OF ELECTROCHEMICAL TECHNIQUES

It is evident from section 5.2 that the screening of inhibitors was done through different techniques. Now, there arises a question of whether the efficiency values that are obtained from various methods give similar results or not. This section deals with reviewing the different methods that were used in inhibitor screening and actively look for any correlations and the discrepancies that arise from calculation of inhibitor efficiencies. The Table 5.2 summarizes the characteristics and limitations of the methods. A graphical representation of the inhibitor efficiencies calculated from PDP, EIS and LPR is shown in the Figure 5.20 and Figure 5.21 below. The data values for this can also be found in appendix.

Table 5.2: Electrochemical techniques for inhibitor studies [15–17]

Sr. no	Technique	Characteristics	Limitation
1	OCP	Provides information on stability of the system.	Qualitative analysis only. No information on corrosion kinetics or efficiency of inhibition.
2	PDP	Conveys information on corrosion kinetics, behaviour during polarisation, and parameters such as passive zones, pitting potential, tafel slope constants, inhibition efficiencies, etc.	Surface properties alteration due to high polarisation of sample and destructive nature.
3	EIS	Gives information about the protective films formed, analysis of physio-chemical processes that occur on surface.	Affects the stationarity of the experiment as it takes some time to scan the sample, complex systems are difficult to interpret and analyse, requires extra surface analysis to support the results.
4	LPR	Time-resolved technique, does not polarise the sample too much and hence non-destructive.	Suitable for screening only, does not provide information on the surface properties, or systems that have multiple protective layers.

It can be seen from the Figure 5.20, that not all techniques give the same efficiency number for a particular inhibitor. While some inhibitors tend to show similar efficiencies even after analysing through different techniques, others reflect completely different efficiency number. For instance, Cerium compounds such as CN 0.1, CN 1, CCl 0.1, CCl 1 which show consistency in its efficiency and an excellent inhibitive nature(positive efficiency) when analysed through all the techniques but Lithium compounds such as LCO 0.1 exhibits 'inhibitive' nature when analysed through PDP 24, EIS 24, and EIS 2, but shows as an corrosion accelerator(negative efficiency) when analysed through LPR 24 and LPR avg methods. Also, in this case, the inhibitor efficiencies shown from PDP 24, EIS 24, and EIS 2 are not consistent with each other.

Among the organic inhibitors as seen from Figure 5.21, DMTD 1 shows a strong corrosion accelerator if analysed through PDP 24, EIS 24, and LPR 24, but exhibits as a good corrosion inhibitor through EIS 2 and a moderate corrosion inhibitor if analysed through LPR avg. BZT shows good inhibitive characteristics through all methods. An increase in the performance is seen with an increase in concentration for BZT and MBDA. On the other hand, NaMA shows excellent performance as analysed through all the methods.

The relationship between efficiency values obtained from different methods was analysed through a statistical approach by studying the correlation between them. A correlation between any two variables is the property of association of these variables and how they *change* wrt each other. Depending on the variables, the correlation between them can be zero if they are completely unrelated to each other. There exists a positive cor-

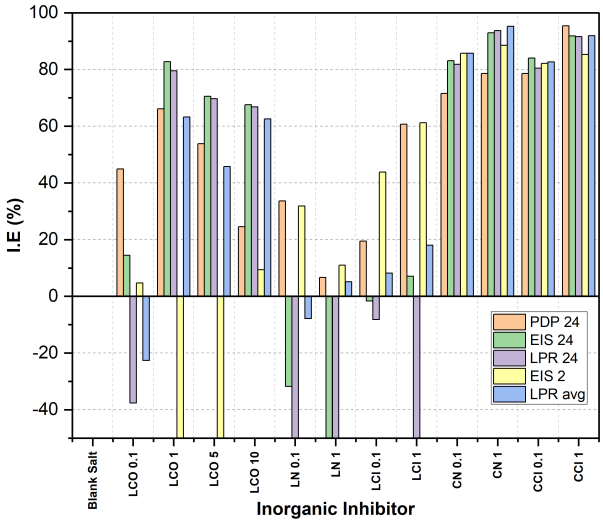

Figure 5.20: An overview of IE of inorganic inhibitors as calculated from different techniques

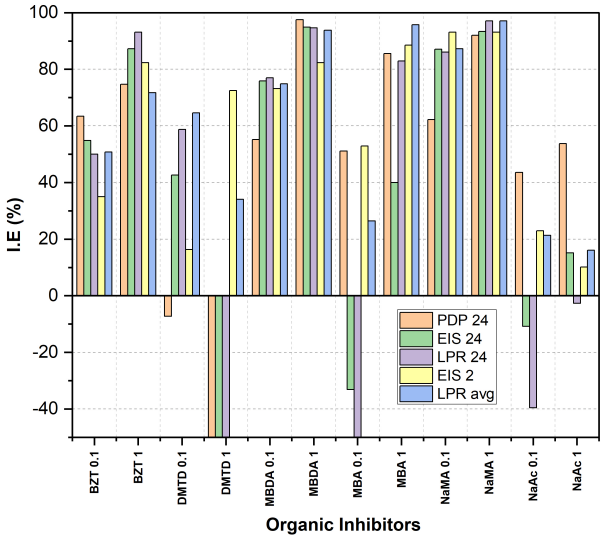

Figure 5.21: An overview of IE of organic inhibitors as calculated from different techniques

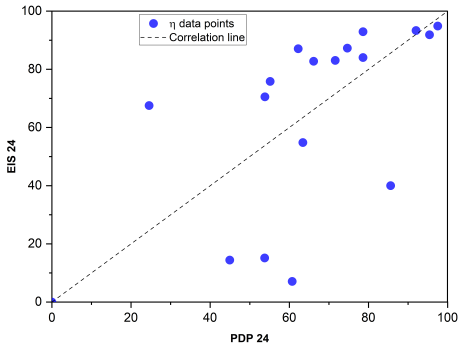

Figure 5.22: An example of scatter plots showing EIS 24 and PDP 24 as independent variables and efficiency obtained from them as data points

relation if both variables increase in the same *manner*. On the contrary, if the variables correlate in a opposing manner, i.e. while one variable tends to increase, the other decreases, then it can be considered as a negative correlation. In our case, the independent variables refers to the different methods (PDP24, EIS 24, LPR 24, EIS 2, LPR avg), through which the efficiency values are calculated.

In a typical correlation scatter plot for representation purpose is shown in Figure 5.22, wherein, the axes represent two variables (in our case, different methods) through which efficiency was calculated and the data points represent the efficiency values. A correlation line goes through the plot, which represents best relationship between variables. Mathematically this is 'y=x' line. When the data points lie in *close* proximity of this line, then it represent *good* correlation between the variables. Whereas, the more scattered or deviating the data points are from the correlation line, the more *unrelated* the variables are [62].

While the scatter plots show the correlation between variables qualitatively, a quantitative analysis of the correlation between experiments can be done by a statistical tool called a Pearson's correlation. It is a method that measures the degree of correlation of *relatedness* between two variables. This particular statistical tool estimates the tendency with which two variables increase or decrease. This coefficient which ranges through -1 to +1, denotes the relationship between variables, with ideal values of -1 denoting a strong negative correlation, or +1 denoting a strong positive correlation or 0, if there is no correlation. Before any correlation is analysed, it is assumed that there exists no correlation between variables. This is also called as the null hypothesis. P-value of a simple correlation tells how likely it is to get a null hypothesis. So, lower is the p value, it is less likely to get a result if the null hypothesis is true. Thus, the p-values associated to any correlation denotes if the correlation is significant or not. Usually, p-values less than 0.05 denotes that the correlation is significant [62, 63].

The correlation between methods was represented in a correlation matrix as shown in Figure 5.24. It is a triangular matrix wherein each cell represents the correlation as-

sociated to the pair-wise method. In the lower triangular matrix, red circle represents a positive correlation and blue circle represents a negative correlation. The significance of a correlation is denoted by number of asterisks (*) in a circle, with higher asterisks denoting more significant correlation. It is based on p-values. The bigger the circle, higher is the correlation coefficient. Correlation coefficients for the pair-wise methods are given in the upper triangular matrix from a scale of -1 to +1.

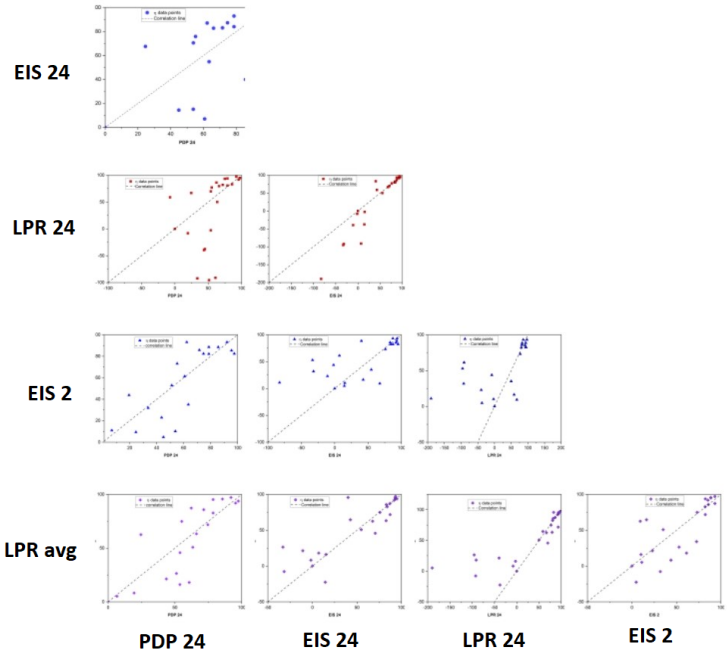

Figure 5.23: Scatter plots showing qualitatively the correlation among different methods for obtaining inhibitor efficiencies.

From the scatter plots in Figure 5.23 it can be observed qualitatively that there is a very weak correlation between EIS 2 and other methods. For most of the data points tend to deviate or scatter from the correlation line. This can also be noted from Figure 5.20 and Figure 5.21, wherein data points from EIS 2 show very contrasting numbers for any particular inhibitor compared to other techniques. Hence, it can be said that EIS 2 has weak correlation with other methods. This can also be seen from the Figure 5.24. It has a correlation coefficient close to zero, and a negative one, which suggests that the data-set from this method could be less reliable and does not show any significance. On the other hand, the scatter plots between LPR 24, EIS 24 and PDP 24 show very good correlation and significance, with coefficients of 0.92, 0.83, and 0.97 indicating a strong relationship. This makes sense because at a specific time, all the methods would give similar values of efficiencies as calculated from electrochemical parameters, j_{corr} in case of PDP 24 and R_p in case of LPR 24 and EIS 24 and considering that these parameters are

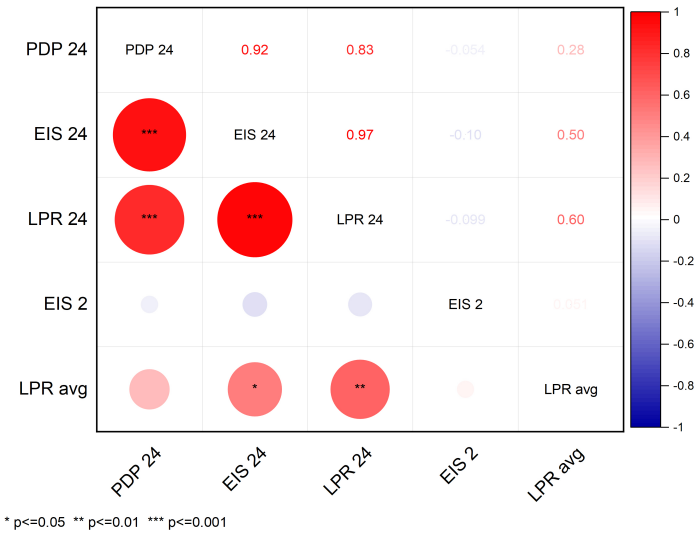

Figure 5.24: Correlation matrix indicating the correlation coefficients between methods.

indeed related to each other. Interestingly, LPR avg with other methods (EIS 24, LPR 24 and PDP 24), show that data points do form a cluster at higher efficiencies. They lie close to the correlation line. Specifically, LPR avg exhibits a good positive correlation with LPR 24 with a correlation coefficient of 0.60. This suggests that the R_p as calculated from the LPR avg technique shows a good trend with other methods and is thus definitive.

5.5. DISCUSSIONS

Among the compounds that were tested, lithium and cerium were examined for common set of anions, such as carbonate, nitrate and chloride. It was seen that CCO was insoluble in water, even at as low as 0.1mM concentration, which restricts its use as corrosion inhibitor for AA2024-T3. On the other hand, compared to the lithium anions, cerium anions were seen to be much more effective, stable and exhibiting similar performance characteristics as analysed through different electrochemical methods. On analysing the onset of pitting which is characterised by the pitting potential, it was seen that most of the inhibitors exhibit similar values. This may be an indicative that inhibitors do not influence the onset of pitting, rather lower the corrosion potential instead, thereby increasing the passive range. Also, contrasting characteristics can be seen from the inhibitor performance and passive range values. While LCl showed excellent passive range, it was seen to be fairly effective. At the same time, CN 1 and MBDA 1, that showed excellent performance through the PDP experiment, exhibited lower passive range values.

Inhibition is a dynamic process, i.e it evolves in time. This can be seen from the time dependent characteristics from the LPR measurements. For organic inhibitors, they adsorb chemically or physically to the surface, and with prolong exposure times, the adsorption may become stronger. For inorganic inhibitors, the compounds gets detached from anion and form hydroxides on the surface. Due to the non-steady state properties, it becomes difficult to continuously monitor the ongoing changes in the system. But LPR serves the necessary purpose. The time dependent characteristics show that until the generally, until the 6^{th} hour, most of the inhibitors showed unstable behaviour. Subsequently, it follows that any measurement for inhibitor efficiency below this hour will lead to ambiguous results. The fact that inhibition efficiencies as calculated from the EIS at 2^{nd} hour shows some compounds such as LCO 1 and LCO 5 to be acting as corrosion accelerators, which is not the case. At the same time, DMTD was seen to have inhibitive properties although poor characteristics. Due to this time dependency, it becomes difficult to rely on the performance characteristics when analysed at this hour. This can also be noted from the poor correlation of inhibitor efficiency as calculated from EIS at the 2^{nd} hour with the other methods. 'p' values denote the significance of the correlation. EIS 2 showed higher p-values than 0.05, which would indicate that the there is a chance that our correlation is not significant and we are forcefully trying to get a correlation among them. Studying a large amount of inhibitors will probably make correlations statistically clearer and significant.

The corrosion mechanism and dynamics of the corrosive activities of this particular alloy is still a matter of research due to its complex microstructure. Unlike any other metals, that exhibit uniform corrosion, AA2024-T3 shows localised forms of corrosion due to the IMP present in it. Hence, the corrosion rate in the case of AA2024-T3 is not uniform. With the presence of inhibitors, the kinetics can be slowed down, but considering only the kinetic parameters while selecting an inhibitor would rather be incomplete. Inhibitor efficiency metric is a kinetic parameter and is highly non linear. The scatter plots show a common feature, that is, more data points are clustered at higher efficiency numbers. Due to this non linear property, even a small increase in the polarisation resistance for lower values increases the efficiency, while for the higher values,

even a large increase in polarisation resistance does not increase the efficiency as much. Hence, large data points gets clustered at higher efficiencies. A new metric thus needs to be developed that has a linear nature. At the same time, calculation of inhibitor efficiencies is a subjective task. As seen from the screening process, different techniques give different numbers as inhibition efficiencies for the same compound. Hence, when it comes to evaluating the performance of inhibitors, conducting different experiments and comparing them is a crucial task.

The most important aspect while screening is the reproducibility of the experiment. A good reproducibility can be achieved up to an extent through uniform sample preparation and keeping the experimental parameters constant. Yet, it was seen that, it cannot be fully accomplished. A possible reason could be that the pit density on the surface of the alloy can make considerable changes in corrosion behaviour even though tested for the same inhibitor and under similar experimental conditions.

6

CONCLUSIONS

The main aim of this research was to study environmentally friendly compounds that could be used as corrosion inhibitors for AA2024-T3.

- Electrochemical techniques reveal that among the selected inorganic compounds, lithium compounds could not significantly reduce the corrosion current as much as cerium compounds. Specifically, Cerium chloride was seen to be reducing the corrosion current density as low as up to one order of magnitude. However, the barrier properties of lithium compounds were seen to be higher. Pitting potential for samples exposed to inhibitors was seen to be almost similar to that of blank sample, suggesting that inhibitors had negligible effect on the onset of pitting, but rather changed the corrosion potential values, thus affecting the barrier properties. Time dependent study revealed that 1mM Cerium chloride had a stable behaviour. On the other hand,1mM 2-Mercaptobenzimidazole was seen to have reduced the corrosion current the most, and at the same time, revealed stable characteristics during 24 hours. But 1mM Na-Mercaptoacetate was seen to have higher R_p values than 1mM Mercaptobenzimidazole from 6 hours with a stable behaviour until 24 hours. 2,5-Dimercapto-1,3,4-Thiadiazole was seen to be acting as a strong corrosion accelerator after 6 hours.
- Inhibitors are characterised by their inhibitor efficiency. A screening of inhibitors was done through different methods. It was seen that 1mM Cerium chloride and 1mM Cerium Nitrate were the most effective ones, among the inorganic inhibitors. They showed excellent kinetic parameters as compared to lithium compounds, and more or less stable time dependent characteristics. Organic compounds on the other hand were seen to have better inhibitive and time dependent properties. The best ones in terms of performance were 1mM Na-Mercaptoacetate and 1mM 2-Mercaptobenzimidiazole. The organic inhibitors were seen to have stable behaviour after 6 hours of exposure.
- In-situ and ex-situ FTIR measurements on samples exposed to 1mM Na Mercaptoacetate showed carboxyl peaks and surface hydroxylation. Thiol group was seen

to be absent which denoted the adsorption could have taken place through the carboxyl group. However, XPS measurements confirmed that sulphur is present on the surface, in low amounts. 1mM Cerium Nitrate when studied through XPS showed the presence of cerium oxides on the surface, which was interesting considering the low amount of cerium nitrate.

- The different methods that were used to calculate the inhibitor efficiency had some correlations between them. Data points from most of the methods were observed to be clustering at higher efficiencies. Measurements at the 2^{nd} hour were seen not to be significant, with EIS 2 method showing no correlation with other methods. This is because the corrosion activities were seen to be ongoing until a long time of almost 6 hours which was evident from the variations in the R_p values. So any measurement and analysis about efficiency until this hour might lead to contrasting numbers. Measurements at the 24^{th} hour did have excellent correlations among them. The integral average technique had a positive and good correlation with other methods.

To sum up, it can be noted that not always inhibitor efficiency is a reliable factor when it comes to selection of inhibitors for AA2024-T3. A possible reason is because inhibitor efficiency as a metric is highly non-linear. Also, aluminium does not corrode uniformly, but shows pitting, unlike other substrates, which exhibit uniform corrosion. The corrosion kinetics in this case, differs, which makes it difficult to assign a number.

7

FUTURE SCOPE AND RECOMMENDATIONS.

While the current work was focused on the selection and screening of corrosion inhibitors, a lot of work can be still done focusing on the depth of the topic. Some recommendations for future studies are given below:

1. The irreversibility aspects of corrosion inhibitors play an important role in studying how reliable these inhibitors are in a system. Irreversibility is a property due to which the inhibitor retains its protective properties even when the concentration decreases. The compounds can be tested for their irreversibility nature.

2. As seen from the results, there exists discrepancies between various methods that can be implemented to calculate inhibitor efficiencies. Inhibitor efficiency thus becomes skeptical to rely on. A new mathematical and numerical tool can be developed, that takes into account all of the characteristics of an inhibitor, which could prove to be more reliable and consistent.

3. The current work followed an experimental approach. The data points obtained from experiments can be used to create machine learning models and algorithms to predict and screen appropriate inhibitors, thereby reducing the man-hours involved in experiments and data analysis.

4. Literature still lacks about getting to know the exact mechanism of inhibition for organic and inorganic compounds. Although a common phenomena is that inhibitor forms a protective layer on the surface, the effect of chemical structures of inhibitors on the surface properties still needs to be addressed. An EIS investigation supported by localised measurements can be done to identify the interface properties. Localised techniques such as Atomic Force Micrography and Scanning Vibrating Electrode Technique can be implemented to study the microscopic changes on the surface due to presence of inhibitors.

5. Due to time constraints, the current research did not consider the effect of mixed inhibitors. This is an interesting area because it has been shown in the past that mixed inhibitors show excellent inhibitive properties. Moreover, the other characteristics were seen to be totally different from the individual ones. This may lead to development of new and effective synthetic compounds that could be used as inhibitors.

6. Corrosion in aluminium is a complex process, which is still under investigating process. Another interesting phenomena that can be studied is the role of intermetallic particles in the corrosion inhibition of AA2024-T3.

REFERENCES

[1] *Aloha Airlines Flight 243,* (2021), page Version ID: 1026802578.

[2] T. Herald-Dispatch, *Gallery: Historical photos of the 1967 collapse of the Silver Bridge,* .

[3] J. Tao, *Surface composition and corrosion behavior of an Al-Cu alloy*, Ph.D. thesis (2016).

[4] W. Cassada, J. Liu, and J. Staley, *Aluminum alloys for aircraft structures,* Advanced Materials and Processes **160**, 27 (2002).

[5] S. He, *Lithium and cerium based sol-gel coatings for corrosion protection of AA2024-T3,* , 68.

[6] K. A. Yasakau, M. L. Zheludkevich, S. V. Lamaka, and M. G. S. Ferreira, *Mechanism of Corrosion Inhibition of AA2024 by Rare-Earth Compounds,* The Journal of Physical Chemistry B **110**, 5515 (2006).

[7] K. Yasakau, M. Zheludkevich, and M. Ferreira, *Role of intermetallics in corrosion of aluminum alloys. Smart corrosion protection,* in *Intermetallic Matrix Composites* (Elsevier, 2018) pp. 425–462.

[8] P. Visser, H. Terryn, and J. M. C. Mol, *Aerospace Coatings,* in *Active Protective Coatings*, Vol. 233, edited by A. E. Hughes, J. M. Mol, M. L. Zheludkevich, and R. G. Buchheit (Springer Netherlands, Dordrecht, 2016) pp. 315–372, series Title: Springer Series in Materials Science.

[9] Zaki Ahmad, *Principles of Corrosion Engineering and Corrosion Control*, 06 (IChemE publications, 2006) p. 42.

[10] O. Gharbi, S. Thomas, C. Smith, and N. Birbilis, *Chromate replacement: what does the future hold?* npj Materials Degradation **2**, 12 (2018).

[11] B. N. Popov, *Basics of Corrosion Measurements,* in *Corrosion Engineering* (Elsevier, 2015) pp. 181–237.

[12] *Basics of EIS: Electrochemical Research-Impedance,* .

[13] C. G. and A. F., *Corrosion Inhibitors – Principles, Mechanisms and Applications,* in *Developments in Corrosion Protection*, edited by M. Aliofkhazraei (InTech, 2014).

[14] F. C. Campbell, *Manufacturing technology for aerospace structural materials*, 1st ed. (Elsevier, Amsterdam ; Boston, 2006).

[15] P. Taheri, I. Milošev, M. Meeusen, B. Kapun, P. White, A. Kokalj, and A. Mol, *On the importance of time-resolved electrochemical evaluation in corrosion inhibitor-screening studies,* npj Materials Degradation **4**, 12 (2020).

[16] P. Visser, Y. Liu, X. Zhou, T. Hashimoto, G. E. Thompson, S. B. Lyon, L. G. J. van der Ven, A. J. M. C. Mol, and H. A. Terryn, *The corrosion protection of AA2024-T3 aluminium alloy by leaching of lithium-containing salts from organic coatings,* Faraday Discussions **180**, 511 (2015).

[17] P. Visser, H. Terryn, and J. Mol, *On the importance of irreversibility of corrosion inhibitors for active coating protection of AA2024-T3,* Corrosion Scienglishce **140**, 272 (2018).

[18] *PubChem: National Center for Biotechnology Information,* https://pubchem.ncbi.nlm.nih.gov/ (), Accessed: June, 2021.

[19] *Chemical Book,* https://www.chemicalbook.com/ProductIndex_EN.aspx (), Accessed: June, 2021.

[20] D. A. Jones, *Principles and prevention of corrosion,* 2nd ed. (Prentice Hall, Upper Saddle River, NJ, 1996).

[21] E. McCafferty, *Introduction to Corrosion Science* (2010) pp. 1–575.

[22] M. G. Fontana and N. D. Greene, *Corrosion engineering / Mars G. Fontana, Norbert D. Greene*, 2nd ed. (McGraw-Hill New York, 1978) pp. xiii, 465 p. :.

[23] N. Perez, *Electrochemistry Science and Corrosion* (2016) p. Second Edition.

[24] B. N. Popov, *Springer Science+Business Media, LLC 2010* (2015) pp. 1–774.

[25] A. Mol and P. Taheri, *Ms43120: Corrosion engineering,* University Lecture, Technical University of Delft (2021).

[26] G. Palanisamy, *Corrosion Inhibitors* (IntechOpen, 2019) publication Title: Corrosion Inhibitors.

[27] *Evaluation of corrosion inhibitors,* .

[28] Y. Gonzalez-Garcia, *Ms43220: Corrosion science,* University Lecture, Technical University of Delft (2020).

[29] J. R. Kissell, S. G. Pantelakis, and G. N. Haidemenopoulos, *Aluminum and Aluminum Alloys,* in *Handbook of Advanced Materials*, edited by J. K. Wessel (John Wiley & Sons, Inc., Hoboken, NJ, USA, 2004) pp. 321–463.

[30] H. Kamoutsi, G. Haidemenopoulos, V. Bontozoglou, and S. Pantelakis, *Corrosion-induced hydrogen embrittlement in aluminum alloy 2024,* Corrosion Science **48**, 1209 (2006).

[31] Z. Szklarska-Smialowska, *Pitting corrosion of aluminum,* Corrosion Science **41**, 1743 (1999).

[32] P. Campestrini, E. van Westing, H. van Rooijen, and J. de Wit, *Relation between microstructural aspects of AA2024 and its corrosion behaviour investigated using AFM scanning potential technique,* Corrosion Science **42**, 1853 (2000).

[33] M. Shao, Y. Fu, R. Hu, and C. Lin, *A study on pitting corrosion of aluminum alloy 2024-t3 by scanning microreference electrode technique,* .

[34] K. Yasakau, J. Tedim, M. Zheludkevich, and M. Ferreira, *Smart self-healing coatings for corrosion protection of aluminium alloys,* in *Handbook of Smart Coatings for Materials Protection* (Elsevier, 2014) pp. 224–274.

[35] A. Kosari, *Corrosion and Corrosion Inhibition Studies of Aerospace Aluminium Alloys at the Nanoscale using TEM Approaches*, Ph.D. thesis, Delft University of Technology (2021).

[36] L. Coelho, D. Cossement, and M.-G. Olivier, *Benzotriazole and cerium chloride as corrosion inhibitors for AA2024-T3: An EIS investigation supported by SVET and ToF-SIMS analysis,* Corrosion Science **130**, 177 (2018).

[37] *DoITPoMS - TLP Library The Nernst Equation and Pourbaix Diagrams - Construction of a Pourbaix Diagram,* ().

[38] V. S. Jayalakshmi, Muralidharan, *INHIBITORS FOR ALUMINIUM CORROSION IN AQUEOUS MEDIUM,* Corrosion Reviews **15**, 26 (1997).

[39] E. Charitidou, G. Papapolymerou, G. N. Haidemenopoulos, N. Hasiotis, and V. Bontozoglou, *Characterization of trapped hydrogen in exfoliation corroded aluminum alloy 2024,* Scripta Materialia **41**, 1327 (1999).

[40] R. G. Kelly, J. R. Scully, D. Shoesmith, and R. G. Buchheit, *Electrochemical Techniques in Corrosion Science and Engineering*, 0th ed. (CRC Press, 2002).

[41] *Corrosion Inhibition: Theory and Practice,* in *Green Corrosion Inhibitors* (John Wiley & Sons, Inc., Hoboken, NJ, USA, 2011) pp. 139–166.

[42] *chromium | Uses, Properties, & Facts | Britannica,* .

[43] L. Xia and R. L. McCreery, *Chemistry of a Chromate Conversion Coating on Aluminum Alloy AA2024-T3 Probed by Vibrational Spectroscopy,* Journal of The Electrochemical Society **145**, 3083 (1998).

[44] J. D. Ramsey and R. L. McCreery, *In Situ Raman Microscopy of Chromate Effects on Corrosion Pits in Aluminum Alloy,* Journal of The Electrochemical Society **146**, 4076 (1999).

[45] G. S. Frankel and R. L. McCreery, *Inhibition of Al Alloy Corrosion by Chromates,* The Electrochemical Society Interface **10**, 34 (2001).

[46] G. O. Ilevbare, J. R. Scully, J. Yuan, and R. G. Kelly, *Inhibition of Pitting Corrosion on Aluminum Alloy 2024-T3: Effect of Soluble Chromate Additions vs Chromate Conversion Coating,* CORROSION **56**, 227 (2000).

[47] C. Pellerin and S. Booker, *Reflections on hexavalent chromium: Health hazards of an industrial heavyweight,* Environmental health perspectives **108**, A402 (2000).

[48] M. Meeusen, P. Visser, L. Fernández Macía, A. Hubin, H. Terryn, and J. Mol, *The use of odd random phase electrochemical impedance spectroscopy to study lithium-based corrosion inhibition by active protective coatings,* Electrochimica Acta **278**, 363 (2018).

[49] D. M. D. L. Escalera, J. J. Ramos-Hernandez, E. Porcayo-Palafox, J. Porcayo-Calderon, J. G. Gonzalez-Rodriguez, and L. Martinez-Gomez, *Effect of [nd.sup.3+] ion concentration on the corrosion resistance of api x70 steel in chloride-rich environments,* Advances in Materials Science and Engineering **2018** (2018), 10.1155/2018/9328317.

[50] R. Catubig, A. Hughes, I. Cole, B. Hinton, and M. Forsyth, *The use of cerium and praseodymium mercaptoacetate as thiol-containing inhibitors for AA2024-T3,* Corrosion Science **81**, 45 (2014).

[51] M. Gobara0 and H. Kamel, *Corrosion behaviour of aa2024 coated with an acid-soluble collagen/hybrid silica sol-gel matrix,* Proceeding of the 7th ICEE Conference 27-29 May 2014 (2014).

[52] L. I. Fockaert, T. Würger, R. Unbehau, B. Boelen, R. H. Meißner, S. V. Lamaka, M. L. Zheludkevich, H. Terryn, and J. M. Mol, *Atr-ftir in kretschmann configuration integrated with electrochemical cell as in situ interfacial sensitive tool to study corrosion inhibitors for magnesium substrates,* Electrochimica Acta **345**, 136166 (2020).

[53] D. K. Kozlica, A. Kokalj, and I. Milošev, *Synergistic effect of 2-mercaptobenzimidazole and octylphosphonic acid as corrosion inhibitors for copper and aluminium – an electrochemical, xps, ftir and dft study,* Corrosion Science **182**, 109082 (2021).

[54] Z. Tang, *A review of corrosion inhibitors for rust preventative fluids,* Current Opinion in Solid State and Materials Science **23**, 100759 (2019).

[55] K. Xhanari, M. Finsgar, M. Knez Hrncic, U. Maver, Z. Knez, and B. Seiti, *Green corrosion inhibitors for aluminium and its alloys: a review,* RSC Advances **7**, 27299 (2017).

[56] M. Gobara, A. Baraka, R. Akid, and M. Zorainy, *Corrosion protection mechanism of ce 4+ /organic inhibitor for aa2024 in 3.5% nacl,* RSC Advances **10**, 2227 (2020).

[57] P. J. . Denissen, S. J. Garcia, and P. J. Denissen, *Reducing subjectivity in eis interpretation of corrosion and corrosion inhibition processes by in-situ optical analysis,* (2018), 10.1016/j.electacta.2018.10.018.

[58] *Corrosion Inhibitor Testing - Home,* ().

[59] Y. Leng, *Materials characterization: Introduction to microscopic and spectroscopic methods: Second edition,* Materials Characterization: Introduction to Microscopic and Spectroscopic Methods :Second Edition , 1 (2013).

[60] T. Scientific, *Introduction to fourier transform infrared spectroscopy,* .

[61] P. V. der Heide, *X-ray photoelectron spectroscopy : an introduction to principles and practices* (Wiley-Blackwell, 2012).

[62] S. Boslaugh and P. A. Watters, *Statistics in a nutshell* (O'Reilly Media,, 2012) pp. 173–191.

[63] D. Nettleton, *Chapter 6 - selection of variables and factor derivation,* in *Commercial Data Mining*, edited by D. Nettleton (Morgan Kaufmann, Boston, 2014) pp. 79–104.

A

MATERIAL AND EXPERIMENT INPUT PARAMETERS

This chapter presents the inhibitor compounds physical and experimental properties. Along with, the input experimental parameters that were set for electrochemical experiments is provided.

Table A.1: Solubility limits for the inhibitor compounds as adapted from Chemical handbook solubility charts [18, 19]

Inhibitor compound	**Molecular weight (g/mol)**	**Solubility limit (g/100ml)**	**Remarks**
NaCl	58.44	36.0	Extremely soluble
Li_2CO_3	73.89	1.3	Slightly soluble
$LiNO_3$	68.95	70.1	Extremely soluble
LiCl	42.39	8.5	Moderately soluble
$Ce(NO_3)_3.6H_2O$	434.23	17.5	Moderately soluble
$CeCl_3.7H_2O$	372.58	≈100	Extremely soluble
$CeCO_3.1H_2O$	460.27	<0.1	Practically insoluble
Benzatriazole	119.12	≈2	Slightly soluble
Sodium Acetate	136.08	46.5	Extremely soluble
2,5 DiMercapto 1,3,4 Thiadiazole	150.25	≈2	Slightly soluble
2-Mercaptobenzimidiazole	150.2	<1	Insoluble
2-Mercaptobenzoate	176.16		
Sodium Mercaptoacetate	114.10	≈20	Extremely soluble

Table A.2: Experiment parameters initialization and values

OCP		LPR		EIS		PDP	
Parameter	Value	Parameter	Value	Parameter	Value	Parameter	Value
tR (h:m:s)	0:10:0,0000	tR (h:m:s)	0:00:0,0000	Mode	Single sine	tR (h:m:s)	0:10:0,0000
dER/dt (mV/h)	0,0	dER/dt (mV/h)	0,0	E (V)	0,0000	dER/dt (mV/h)	5,0
dER (mV)	0,00	dER (mV)	0	vs.	Eoc	dER (mV)	5
dtR (s)	0,5000	dtR (s)	0,0000	tE (h:m:s)	0:00:0,0000	dtR (s)	1,00
E range min (V)	-10,000	dE/dt	0,500	record	0	dE/dt	0,500
E range max (V)	10,000	dE/dt unit	mV/s	dI	0,000	dE/dt unit	mV/s
		Ei (V)	-0,010	unit dI	mA	Ei (V)	-0,250
		vs.	Eoc	dt (s)	0,000	vs.	Eoc
		EL (V)	0,010	fi	10,000	EL (V)	0,250
		vs.	Eoc	unit fi	kHz	vs.	Eoc
		record		ff	10,000	record	
		dI	0,000	unit ff	mHz	dI	0,000
		unit dI	µA	Nd	10	unit dI	µA
		tI (s)	0,0000	Points	per decade	tI (s)	0,00
		step percent	25	spacing	Logarithmic	step percent	25
		N	5	Va (mV)	10,0	N	5
		E range min (V)	-10,000	pw	0,10	E range min (V)	-10,000
		E range max (V)	10,000	Na	3	E range max (V)	10,000
		I Range	Auto	corr	0	I Range	Auto
		I Range min	10 mA	E range min (V)	-10,000	I Range min	10 mA
		I Range max	10 mA	E range max (V)	10,000	I Range max	10 mA
		I Range init	10 mA	I Range	Auto	I Range init	10 mA
		Bandwidth	8	Bandwidth	8	Bandwidth	8
				nc cycles	0		
				goto Ns'	0		
				nr cycles	0		
				inc. cycle	0		

B

EXPERIMENT DATA POINTS

This chapter presents all the data points that were analysed from the electrochemical experiments. The data files can be provided if necessary upon request.

Table B.1: LPR data of inorganics

Sample	Basic salt		Li2CO3 0.1mM		Li2CO3 1mM		Li2CO3 5mM		Li2CO3 10mM	
Time(hrs)	Mean	Std Dev	Mean	Std Dev	Mean	Std Dev	Mean	Std Dev	Mean	Std Dev
0.5	12938.6	1127.962	15824.8	3614.714	8011.333	1076.045	1637	268.7545	5316.2	2286.823
1	15894.2	4612.491	15790.5	1433.444	6882.333	2299.636	3650	1315.63	10000.2	3283.175
2	17338.6	4433.077	19000.4	2234.212	2595.667	1152.962	5276.667	1478.246	15862.6	6149.947
3	19843.2	6797.639	18599.6	3800.907	4187.333	215.1333	10100.33	4089.012	29152.2	13221.65
6	23425	6731.221	14190.6	2670.714	13967.33	7515.534	15648.67	2159.542	46564.4	26347.42
12	17611.8	5592.475	13492.4	2175.546	52845.67	8480.892	32163	9923.064	54441.8	14350.76
18	12371.2	3646.379	10984.6	1620.131	79939.67	31292.66	51373	10873.7	61975	15013.77
24	15744.6	3565.702	14362.4	2489.499	88363.33	39308.34	57211.33	14314.76	47110.8	16471.35
Trapezoidal	13.78136	3.493676	11.2426	0.666076	37.53376	7.082109	25.39332	5.455273	36.78362	11.19298

Table B.2: LPR data of inorganics

Sample	Basic salt		LiNO3 0.1mM		LiNO3 1mM		LiCl 0.1mM		LiCl 1mM	
Time(hrs)	Mean	Std Dev	Mean	Std Dev	Mean	Std Dev	Mean	Std Dev	Mean	Std Dev
0.5	12938.6	1127.962	20692.67	2817.259	21089.25	7279.976	29065.33	10230.13	20609.33	6003.484
1	15894.2	4612.491	22388	4955.987	32679.25	17297.08	26258.33	7776.105	27473	9428.854
2	17338.6	4433.077	30370.67	13686.87	24616.5	6560.016	31555	10071.08	36925.67	16800.2
3	19843.2	6797.639	30051	5450.63	21685.5	3435.407	26253.67	13912.47	35368	25340.02
6	23425	6731.221	16131.67	4118.388	21048.5	10554.39	18365.67	2072.004	16415	5512.632
12	17611.8	5592.475	13357.33	2298.828	8442.5	4096.389	18473.33	4112.534	26045	12762.24
18	12371.2	3646.379	11528.33	2253.146	19305.5	19989.16	11809.33	1143.805	11417.33	1755.533
24	15744.6	3565.702	10022	416.3232	18809.5	14487.81	18205.33	6482.732	16605.67	7819.728
Trapezoidal	13.78136	3.493676	12.78205	1.583621	14.5242	4.702803	15.00942	3.274551	16.81459	5.358798

Table B.3: LPR data of inorganics

Sample	Basic salt		CeNO3 0.1mM		CeNO3 1mM		CeCl3 0.1mM		CeCl3 1mM	
Time(hrs)	Mean	Std Dev	Mean	Std Dev	Mean	Std Dev	Mean	Std Dev	Mean	Std Dev
0.5	12938.6	1127.962	103647.5	57894.4	222547.3	161109	165306.7	161226.6	91331	71275.64
1	15894.2	4612.491	70339	9497.615	277550.3	266703.2	97407	49374.71	139668.7	38436.52
2	17338.6	4433.077	174284.5	94941.98	232718.3	69544.56	125338.5	106939.3	172260.3	86575.12
3	19843.2	6797.639	127645	47601.88	186310.3	75485.28	56174.33	35659.79	158544.7	57694.53
6	23425	6731.221	128158.3	48391.6	258572	170608.7	121677.3	83619.66	184865.7	100945.7
12	17611.8	5592.475	138528.8	80741.55	684530	634810.3	89946.33	54667.82	212498	30734.5
18	12371.2	3646.379	98658.25	32882.99	287788.7	60694.83	100500.7	70989.6	272750.3	87577.79
24	15744.6	3565.702	109875	62072.18	222600.3	69206.64	99133.67	67705.59	230916	39629.31
Trapezoidal	13.78136	3.493676	96.81704	40.22161	287.4919	186.5759	79.69538	45.50991	170.3788	47.89479

Table B.4: LPR data or organics

Sample and time	Basic salt		Benzatriazole 0.1mM		Benzatriazole 1mM		2,5 Dimercaptobenzimidiazole 0.1mM		2,5 Dimercaptobenzimidiazole 1mM	
Time(hrs)	Mean	Std Dev	Mean	Std Dev	Mean	Std Dev	Mean	Std Dev	Mean	Std Dev
0.5	12938.6	1127.962	17354.25	4759.428	42847	17478.4	167858.6667	146835.1	256419	15529.48
1	15894.2	4612.491	21066.25	4860.577	53805.33	24653.97	42101.33333	37376.14	173013	34296.09
2	17338.6	4433.077	20362.75	6291.037	60084.33	21125.54	16213.5	311.8341	129198	61593.24
3	19843.2	6797.639	26786.75	5024.451	60672	29951.57	35030.33333	13290.63	47689	24723.28
6	23425	6731.221	35736.25	11308.65	61636.33	31185.68	50700.33333	29805.21	3994.5	444.7702
12	17611.8	5592.475	40489.75	14915.77	58253.33	30126.03	58825.5	42065.08	3525.5	717.7134
18	12371.2	3646.379	36100.5	13538.01	68772.67	37197.62	46682	30397.11	3261	209.3036
24	15744.6	3565.702	40306.5	15416.78	54177.33	24481.07	30641.5	8401.136	3602.5	552.2504
Trapezoidal Rp	13.78136	3.493676	28.0004	7.627936	48.78417	22.66806	38.90139049	23.11244	20.90218682	5.975227

Table B.5: LPR data of organics

Sample and time	Basic salt		Mercaptobenzimidiazole 0.1mM		Mercaptobenzimidiazole 1mM		Mercaptobenzoate 0.1mM		Mercaptobenzoate 1mM	
Time(hrs)	Mean	Std Dev	Mean	Std Dev	Mean	Std Dev	Mean	Std Dev	Mean	Std Dev
0.5	12938.6	1127.962	69296	14827.66	164918.6667	77220.64	44993.5	9414.795	675638.7	924259.4
1	15894.2	4612.491	51242.3333	22349.68	201448.3333	139675.5	67518	45251.83	359361	453452
2	17338.6	4433.077	60256.3333	8170.113	244640.6667	152913.2	46041.75	18483.35	453015.3	124926.5
3	19843.2	6797.639	48002.3333	10160	205333.3333	133822.5	30832.25	13068.84	232252.3	71070.28
6	23425	6731.221	61460.3333	13502.23	226849.3333	134590.6	28406	7166.391	267311.3	113383.7
12	17611.8	5592.475	76972.3333	62390.42	283837.3333	157754.2	17922.75	6913.429	681412	891862.6
18	12371.2	3646.379	76369.6667	66183.16	315131	175100.9	13329	723.1722	399049.7	520965
24	15744.6	3565.702	70509.6667	70952.17	361851.6667	209131	13343.25	5753.281	125237.7	149873.1
Trapezoidal Rp	13.78136	3.493676	54.8165037	33.1196	221.4633741	122.6402	18.72834	2.952258	320.605	302.2838

Table B.6: LPR data of organics

Sample and time	Basic salt		Sodium Mercaptoacetate 0.1mM		Sodium Mercaptoacetate 1mM		Sodium Acetate 0.1mM		Sodium Acetate 1mM	
Time(hrs)	Mean	Std Dev	Mean	Std Dev	Mean	Std Dev	Mean	Std Dev	Mean	Std Dev
0.5	12938.6	1127.962	158711.3333	95984.06	275775	243421.4	21569.5	6593.605	20670.5	5875.384
1	15894.2	4612.491	159809	69922.19	424423	377694.1	22691.75	6789.358	20998	3185.035
2	17338.6	4433.077	173855.6667	95541.18	447778	309786.5	25102	8008.517	20888.25	2061.766
3	19843.2	6797.639	191252.3333	99360.54	137604.75	10977.41	22554.75	7135.801	21092.5	2589.601
6	23425	6731.221	171903.6667	90764.83	657827.6	550186.7	29895	5676.541	25319.5	5133.137
12	17611.8	5592.475	121923.6667	103161.1	654884.4	561949.6	20286.25	4297.652	17056	2676.835
18	12371.2	3646.379	105053.6667	101070.8	673082.6	592861.2	20430.75	2569.399	21158.25	7348.177
24	15744.6	3565.702	97029.33333	121227.7	594492.6	461499.6	13389.5	1244.985	17885.75	3702.709
Trapezoidal Rp	13.78136	3.493676	108.2399131	78.86864	480.1725827	400.2233	17.51589	2.552647	16.41347	2.370016

Table B.7: EIS data

Inhibitor	EIS 2nd hour kohm-cm2		EIS 24th hour kohm-cm2	
	Mean	Std dev	Mean	Std dev
Basic Salt 0.1M	14.02515	0.699207	13.5621	3.218437
Li2CO3 0.1mM	14.71832	2.023131	15.8501	0.984876
Li2CO3 1mM	1.253474	0.218678	78.74457	0.460035
Li2CO3 5mM	5.279852	1.254678	46.0406	3.4186
Li2CO3 10mM	15.46871	6.699898	41.79821	7.825937
LiNO3 0.1mM	20.57004	5.643896	10.29463	1.904339
LiNO3 1mM	15.75508	3.449755	7.426592	0.696779
LiCl 0.1mM	24.94596	6.296127	13.33891	3.298752
LiCl 1mM	36.15568	-	14.59683	4.861614
Ce(NO3)3 0.1mM	98.49006	64.92225	80.07698	27.8074
Ce(NO3)3 1mM	122.5104	57.57224	191.7785	65.68717
CeCl3 0.1mM	78.51303	39.28439	85.00476	59.12933
CeCl3 1mM	95.40212	6.781519	166.7737	20.97678
Benzotraizole 0.1mM	21.5865	7.011861	30.02135	11.62961
Benzotraizole 1mM	79.3041	53.69697	106.5628	82.55557
2,5 Dimercapto 1,3,4 Thiadiazole 0.1mM	16.76382	4.395517	23.63744	10.01918
2,5 Dimercapto 1,3,4 Thiadiazole 1mM	51.02099	25.05668	2.860357	0.171878
Mercaptobenzimidiazole 0.1mM	52.22549	2.45292	56.15516	54.79476
Mercaptobenzimidiazole 1mM	79.55769	51.28085	265.0874	138.294
Mercaptobenzoate 0.1mM	29.74863	12.77298	10.18692	1.266568
Mercaptobenzoate 1mM	121.8003	120.7024	22.60732	4.395548
Na Mercaptoacetate 0.1mM	203.9527	59.72667	105.0228	108.4297
Na Mercaptoacetate 1mM	202.8773	93.81952	203.4187	111.5067
Na Acetate 0.1mM	18.20279	3.586916	12.24176	1.46249
Na Acetate 1mM	15.60888	3.610765	15.98379	2.154844

Table B.8: PDP datapoints

	Ecorr	Epitt	Passive region	jcorr	Anodic slope	Cathodic slope
Basic Salt 0.1M	-613.47±23.6	-495.21±5.29	118.26±22.72	389.04±164.7	166.62±27.64	138.26±19.01
Li2CO3 0.1mM	-583.64±37.72	-488.61±8.48	95.03±39.61	214.23±109.92	69.07±19.19	71.35±6.65
Li2CO3 1mM	-536.47±26.62	-486.57±8.6	49.9±30.33	131.76±52.91	66.17±42.42	74.77±26.52
Li2CO3 5mM	-840.94±47.56	-	-	179.62±65.09	119.33±17.46	135.2±33.85
Li2CO3 10mM	-747.83±68.25	-	-	293.5±63.86	122.22±19.41	137.22±21.19
LiNO3 0.1mM	-620.87±75.19	-493.84±9.84	127.02±72.59	258.17±134.88	88.97±19.17	80.1±8.07
LiNO3 1mM	-683.43±68.62	-497.01±10.54	90.24±63.8	363.06±226.23	70.53±52.84	41.83±35.07
LiCl 0.1mM	-611.9±64.93	-498.5±18.84	142.84±38.03	313.38±247.38	90.97±54.21	89.9±11.44
LiCl 1mM	-774.01±38.27	-507.1±11.32	20.09±5.36	152.87±56.35	34.73±13.71	9.1±1.95
Ce(NO3)3 0.1mM	-646.82±99.6	-496.65±4.88	194.43±53.61	110.51±56.06	128.55±86.5	116.95±29.96
Ce(NO3)3 1mM	-462.89±12.37	-	-	83.23±15.3	20.9±3.82	197.53±82.28
CeCl3 0.1mM	-650.56±67.89	-493.25±11.51	157.31±56.5	83.23±61.16	144.57±51.65	113.17±38.18
CeCl3 1mM	-569.21±25.65	-490.49±13.31	66.28±41.56	17.83±8.92	52.03±22.93	50±16.25
Benzotraizole 0.1mM	-608.8±71.68	-495.03±11.47	113.78±82.56	142.36±70.59	86.28±35.45	74.9±28
Benzotraizole 1mM	-515.06±65.06	-477.66±8.17	64.84±72.15	98.6±110.9	34.04±27.97	77.22±28.72
2,5 Dimercapto 1,3,4 Thiadiazole 0.1mM	-593.15±59.99	-471.45±18.07	121.7±52.71	417.41±299.79	126.2±45.86	101±25.84
2,5 Dimercapto 1,3,4 Thiadiazole 1mM	-604.56±10.81	-	-	2056.05±533.26	70.15±28.78	99.45±29.49
Mercaptobenzimidiazole 0.1mM	-654.89±56.12	-497.73±1.35	157.16±56.64	174.52±144.1	75.07±16.88	70.03±11.99
Mercaptobenzimidiazole 1mM	-521.26±13.27	-	-	9.77±2.65	25.2±10.16	37.47±15.86
Mercaptobenzoate 0.1mM	-570.19±19.92	-491.26±11.45	78.94±15.49	190.06±26.67	76.04±12.43	76.58±12.96
Mercaptobenzoate 1mM	-513.24±43.08	-457.03±40.14	67.05±17.08	56.05±48.6	53.3±23.18	63.93±12.71
Na Mercaptoacetate 0.1mM	-577.52±63.04	-442.75±51.14	134.77±47.65	146.92±118.92	85.67±14.1	72.3±6
Na Mercaptoacetate 1mM	-571.39±41.45	-432.23±44	124.52±19.9	31.08±18.65	81.72±16.91	75.46±4.67
Na Acetate 0.1mM	-609.59±6.72	-491.84±10.71	117.75±9.37	219.43±29.57	77.88±6.94	69.4±7.99
Na Acetate 1mM	-564.11±28.08	-474.35±11.85	89.77±16.81	179.94±44.66	74.1±11.84	71.38±13.33

Table B.9: Efficiency data as calculated from different methods.

	PDP 24	EIS 24	LPR 24	EIS 2	LPR avg
Blank Salt	0.00	0.00	0.00	0.00	0.00
LCO 0.1	44.94	14.44	-37.60	4.71	-22.58
LCO 1	66.13	82.78	79.54	-1018.90	63.28
LCO 5	53.83	70.54	69.69	-165.64	45.73
LCO 10	24.56	67.55	66.79	9.33	62.53
LN 0.1	33.64	-31.74	-92.30	31.82	-7.82
LN 1	6.68	-82.62	-189.90	10.98	5.11
LCl 0.1	19.45	-1.67	-8.20	43.78	8.18
LCl 1	60.71	7.09	-91.10	61.21	18.04
CN 0.1	71.59	83.06	81.86	85.76	85.77
CN 1	78.61	92.93	93.70	88.55	95.21
CCl 0.1	78.61	84.05	80.50	82.14	82.71
CCl 1	95.42	91.87	91.60	85.30	91.91
BZT 0.1	63.41	54.83	50.02	35.03	50.78
BZT 1	74.66	87.27	93.14	82.31	71.75
DMTD 0.1	-7.29	42.62	58.76	16.34	64.57
DMTD 1	-428.49	-374.14	-436.71	72.51	34.07
MBDA 0.1	55.14	75.85	76.98	73.15	74.86
MBDA 1	97.49	94.88	94.63	82.37	93.78
MBA 0.1	51.15	-33.13	-95.47	52.85	26.41
MBA 1	85.59	40.01	82.89	88.49	95.70
NaMA 0.1	62.24	87.09	86.08	93.12	87.27
NaMA 1	92.01	93.33	97.09	93.09	97.13
NaAc 0.1	43.60	-10.79	-39.57	22.95	21.32
NaAc 1	53.75	15.15	-2.67	10.15	16.04